

1 Estimating the Thermodynamic Contribution of Post-Industrial

2 Warming to Recent Greenland Ice Sheet Surface Mass Loss

Formatted: Font color: Auto

3 Jonathon R. Preece¹, Patrick Alexander^{2,3}, Thomas L. Mote¹, Gabriel J. Kooperman¹,
4 Xavier Fettweis⁴, and Marco Tedesco^{2,3}.

5 ¹Department of Geography, University of Georgia, Athens, 30602, USA.

6 ² Lamont-Doherty Earth Observatory, Columbia University, Palisades, 10964, USA.

7 ³ NASA Goddard Institute for Space Studies, New York, 10025, USA.

8 ⁴Laboratory of Climatology, Department of Geography, SPHERES research unit, University of Liège, Liège, Belgium

9
10 Correspondence to: Jonathon R. Preece (jonathon.preece@uga.edu)

11 **Abstract.** The Greenland Ice Sheet has become the largest single frozen source of global sea level rise following a pronounced
12 increase in meltwater runoff in recent decades. The role of anomalous anticyclonic circulation patterns in facilitating this
13 increase has been widely documented; however, this change in atmospheric circulation has coincided with a rapidly warming
14 Arctic. While amplified Arctic warming has undoubtedly contributed to trends in Greenland's mass loss, the contribution of
15 this shift in background conditions relative to changes in regional circulation patterns has yet to be quantified. Here, we apply
16 the pseudo-global warming method of dynamical downscaling to estimate the contribution of the change in the thermodynamic
17 background state under global warming to observed Greenland Ice Sheet surface mass loss since the turn of the century. Our
18 analysis demonstrates that, had the 2000–2019 sequence of atmospheric circulation occurred under a preindustrial
19 thermodynamic background state, anomalous surface mass loss from the ice sheet would have been reduced by over 62%
20 relative to observations. We show that the change in the thermodynamic environment under amplified Arctic warming has
21 augmented melt of the ice sheet via longwave radiative effects accompanying an increase in atmospheric water vapor content.
22 Furthermore, the thermodynamic contribution to surface mass loss during the record melt years of 2012 and 2019 was less
23 than half that of the long-term average, suggesting that the pronounced mass loss during those two summers was more a result
24 of the anomalous atmospheric circulation than a direct consequence of the long-term warming trend.

Deleted: pivotal

Deleted: at high latitudes

Deleted: recent atmospheric dynamical forcing of the Greenland Ice Sheet ...

Deleted: setting

Deleted: over the exceptional

Deleted: demonstrating a reduced influence during periods of strong synoptic-scale atmospheric forcing.

25 1 Introduction

26 Greenland Ice Sheet mass loss has rapidly accelerated since the turn of the century (Hanna et al., 2014, 2024; Khan et al.,
27 2015; Kjeldsen et al., 2015; Mouginito et al., 2019; Otosaka et al., 2023; The IMBIE Team et al., 2020; Velicogna et al., 2020),
28 becoming the largest single frozen source of global sea level rise and second largest among all sources after thermal expansion
29 of the warming oceans (Cazenave et al., 2018; Horwath et al., 2022). While highly variable, mass loss from the Greenland Ice

Deleted: (GrIS)

Field Code Changed

Deleted: GrIS

40 [Sheet](#) has consistently raised global mean sea level by over 0.5 mm yr⁻¹ in recent decades—a rate that outpaces that of the
 41 Antarctic Ice Sheet (Smith et al., 2020; The IMBIE team et al., 2018; The IMBIE Team et al., 2020) and is approximately
 42 equal to that of all other glaciers combined (Cazenave et al., 2018; Zemp et al., 2019). Estimates place the total contribution
 43 of Greenland at over 10 mm of sea level rise since the 1990s (Mouginot et al., 2019; The IMBIE Team et al., 2020). Moreover,
 44 most of the impact of recent climate change on [total](#) mass balance has yet to be realized, as the timescale at which [ice sheet](#),
 45 dynamics adjust to a climate perturbation is an order of magnitude or greater than that of the surface mass balance (SMB)
 46 response (Box et al., 2022). Recent work conservatively estimates another ~274 mm of committed sea level rise before the [ice](#)
 47 [sheet](#) achieves balance with the current climate state—i.e., even without considering the additional impact of any future
 48 warming scenario (Box et al., 2022).

Deleted: GrIS

Deleted: icesheet

Deleted: GrIS

49
 50 Over Greenland, there has been both an acceleration of solid-ice discharge and a decline in SMB over the past few decades
 51 (van den Broeke et al., 2009a; Mankoff et al., 2019; The IMBIE Team et al., 2020); however, increased runoff has caused
 52 SMB to decline at a rate twice that of the observed increase in dynamic ice loss (Box et al., 2022; Fettweis et al., 2017, 2020;
 53 Mote, 2007; Noël et al., 2017). Consequently, SMB reductions have surpassed discharge as the largest source of mass loss
 54 (Mouginot et al., 2019) and, according to global climate models (GCMs) from CMIP5 and CMIP6, SMB losses are expected
 55 to exceed mass accumulation on their own by the year 2100 unless the most ambitious mitigation efforts are implemented
 56 (Noël et al., 2021).

Deleted: Total mass balance is determined as the SMB—principally, the budget of snow accumulation minus meltwater runoff—less any dynamic loss via solid ice discharge from marine terminating outlet glaciers.

Deleted: from the

Deleted: ice sheet

Deleted: GrIS

Deleted:

Deleted: GrIS

57
 58 This change in [ice sheet](#) surface conditions has been associated with a recent shift in summer atmospheric circulation over the
 59 North Atlantic. The negative trend in SMB has coincided with a more persistently negative North Atlantic Oscillation (NAO)
 60 and an increase in atmospheric blocking episodes over Greenland (Bevis et al., 2019; Fettweis et al., 2013; Hanna et al., 2015,
 61 2016, 2018b, 2022; Hofer et al., 2017). Indeed, previous studies have shown a [statistically](#) significant increase in summer
 62 [Greenland](#) blocking since the turn of the century using a variety of blocking detection methods (Davini and D'Andrea, 2020;
 63 Hanna et al., 2022; Woollings et al., 2018), which has played a key role in encouraging melt via multiple contrasting
 64 mechanisms. For example, the positive trend in surface melt has been [ascribed](#) to the suppression of cloud cover by large-scale
 65 subsidence within the blocking ridge (Hofer et al., 2017). This reduction in cloud cover has allowed for anomalously high
 66 [downward](#) shortwave radiation over the southern ice sheet which, owing to its lower surface albedo, is more sensitive to
 67 changes in shortwave radiation than other regions of the [ice sheet](#) (Hofer et al., 2017; Wang et al., 2019). Other studies,
 68 however, have demonstrated the importance of cloud longwave radiative effects, particularly in regions where albedo is high,
 69 such as the northern ice sheet and over the high-elevation accumulation zone (Gallagher et al., 2018; Lenaerts et al., 2019;
 70 Noël et al., 2019; Orsi et al., 2017; Wang et al., 2019). Strong southerly moisture transport upstream of a blocking anticyclone
 71 in July 2012 supported the formation of low-level cloud cover that produced melt over the highest elevations of the ice sheet
 72 for the first time in over a century (Bennartz et al., 2013; Clausen et al., 1988; Fausto et al., 2016b, a; Mattingly et al., 2018;
 73 Meese et al., 1994; Neff et al., 2014; Nghiem et al., 2012). Additionally, the high-amplitude Omega blocking patterns that

Deleted: stark

Deleted: GrIS

Deleted: GrIS

Deleted: over Greenland

Deleted: .

Deleted: Referred to as Greenland blocks,

Deleted: T

Deleted: these persistent, anomalous anticyclones have

Deleted: of the GrIS

Deleted: GrIS

Deleted: linked

Deleted: Greenland blocking through

Deleted: incoming

Deleted: GrIS

Formatted: Font: 10 pt

Field Code Changed

Field Code Changed

Deleted: (Bennartz et al., 2013; Clausen et al., 1988; Fausto et al., 2016b, a; Mattingly et al., 2018; Meese et al., 1994; Neff et al., 2014; Nghiem et al., 2012)

03 have undergone the greatest increase in recent summers deliver moisture farther poleward, generating above-normal downward
04 longwave radiation over the most northern portions of Greenland (Preece et al., 2022)—conditions which have caused
05 pronounced growth of the ablation zone and spurred a disproportionate increase in runoff from the northern drainages of the
06 ice sheet (Noël et al., 2019).

Deleted: in the region

07
08 A natural question is whether this shift in summer circulation may be a symptom of climate change. At the hemispheric scale,
09 there are several theoretical frameworks that postulate a link between changes in the meridional temperature gradient under
10 Arctic Amplification and more frequent persistent weather extremes (Cohen et al., 2014; Coumou et al., 2018; Francis and
11 Vavrus, 2012), and there is mounting evidence of such a link during summer (Cattiaux et al., 2016; Coumou et al., 2015; Di
12 Capua and Coumou, 2016; Kornhuber and Tamarin-Brodsky, 2021; Vavrus et al., 2017). However, not only have GCMs failed
13 to capture the positive trend in Greenland blocking, they consistently predict a decline in blocking frequency in the region
14 (Delhasse et al., 2021; Hanna et al., 2018a)—a critical source of outstanding uncertainty regarding a causal link between
15 anthropogenic climate change and the observed shift in summer circulation over Greenland. Conversely, the change in the
16 background thermodynamic environment, and its resulting impact on SMB, represents a more robust signal of climate change
17 than the potential dynamical response outlined above. Multiple well-documented radiative feedbacks have helped warm the
18 Arctic at four times the global average rate (Pithan and Mauritsen, 2014; Rantanen et al., 2022; Serreze and Barry, 2011). This
19 constitutes a likely contributor to the nonlinear decline in SMB, as surface melt would be expected to increase in frequency
20 and magnitude in a warmer, more humid atmosphere.

Deleted: Focusing on summer Greenland blocking more specifically, Liu et al. (2016) demonstrated a relationship between reduced Arctic sea ice and anticyclonic conditions over Greenland using both observations and modeling.

Deleted: a discrepancy that constitutes

Deleted: ¶

Deleted: GrIS

Deleted: ,

Deleted: GrIS

21
22 The thermodynamic environment over Greenland is surely influenced by changes occurring more broadly throughout the
23 Arctic. Indeed, Box et al. (2013) linked increased precipitation over Greenland to higher Northern Hemisphere surface air
24 temperature and showed that this statistical relationship was more robust than when considering local near-surface
25 temperatures over Greenland or North Atlantic SST—a result that emphasizes the importance of remotely-sourced heat and
26 moisture to the SMB. However, local sea-surface conditions (SSCs) may also play an important role. Specifically, sea ice
27 reductions over adjacent waters could further contribute to elevated temperatures over Greenland through the water vapor
28 feedback, wherein a warmer atmosphere together with an ice-free ocean increases atmospheric water vapor, which then
29 enhances longwave radiative forcing at the surface (Pithan and Mauritsen, 2014; Trenberth, 2011). One of the more intuitive
30 ways that sea ice loss could impact the ice sheet is through advection of warm, moisture-enriched air from the neighboring
31 seas. Studies have revealed a relationship between changes in sea-ice concentration near Greenland and ice sheet SMB
32 (Pedersen and Christensen, 2019; Rennermalm et al., 2009); however, these studies fail to separate direct marine influence
33 from any indirect effects via alteration of the large-scale circulation by oceanic thermal forcing (Ballinger et al., 2019; Liu et
34 al., 2016) or relationships that might arise as a byproduct of mutual forcing of local sea ice concentration (SIC) and ice sheet
35 melt by the large-scale synoptic setting (Ballinger et al., 2018; Stroeve et al., 2017).

Deleted: While t

Deleted: ,

Deleted: (Pithan and Mauritsen, 2014)

Deleted: Thus, o

Field Code Changed

Deleted: GrIS

Deleted: In investigating such a link,

Deleted: s

Deleted: GrIS

Deleted: affects

Deleted:

Deleted: that might occur

Deleted: GrIS

Deleted: (Ballinger et al., 2018; Stroeve et al., 2017)

Field Code Changed

61 Several modeling efforts have demonstrated minimal contribution from local SSCs during summers of pronounced melt due
62 to the persistent katabatic outflow over the ice sheet acts as a barrier to onshore advection (Hanna et al., 2009, 2014; Noël et
63 al., 2014); however, observational evidence suggests that local SSCs may play an important role earlier in the spring. While
64 melt events during summer and fall are primarily a product of large-scale atmospheric conditions (Ballinger et al., 2019;
65 Hermann et al., 2020; Noël et al., 2014), recent work has identified elevated atmospheric moisture and enhanced downward
66 longwave radiation over the ice sheet approximately one week following sea ice retreat in the Baffin Bay and Davis Strait in
67 years of early melt, suggesting that local sea ice anomalies precondition the ice sheet for early melt onset (Stroeve et al., 2017).

68
69 Disentangling the relative contributions of atmospheric dynamics versus thermodynamics is an intractable problem using
70 observations alone. Previous studies have utilized regional climate models (RCMs) to examine the sensitivity of the SMB to
71 perturbations in SSCs (Hanna et al., 2009, 2014; Noël et al., 2014) or atmospheric thermodynamic fields (Delhasse et al.,
72 2018); however, none of these efforts examined the combined influence of atmospheric and SSCs. Furthermore, these studies
73 either applied arbitrary perturbations to the targeted boundary fields or examined a single melt season and, therefore, did not
74 aim to measure the existent contribution of observed changes in these fields to mass loss.

75
76 Here, we provide an estimate of the relative contributions of dynamical versus thermodynamic change to recent Greenland ice
77 sheet surface mass loss using the pseudo-global warming (PGW) method of dynamical downscaling. The PGW method uses
78 adjusted reanalysis data for the initial and lateral boundary conditions of an RCM (Kawase et al., 2008; Kimura and Kitoh,
79 2007; Schär et al., 1996). To obtain the adjusted boundary conditions, this method applies a climate change perturbation signal
80 that is estimated from GCM output by assuming a linear change in the boundary fields between the control period (i.e., the
81 period of observed reanalysis data) and some alternative period of interest with a contrasting thermodynamic background state
82 (Kawase et al., 2008; Rasmussen et al., 2011; Schär et al., 1996). Thus, the PGW technique effectively isolates the impact of
83 the long-term thermodynamic component of climate change by assuming that the timing and structure of synoptic disturbances
84 along the RCM's boundaries will be the same in the alternative period as during the control (Lackmann, 2015).

85
86 While the PGW method is typically utilized to simulate future conditions, it can also be used to investigate how recent periods
87 of climate or individual weather events would have behaved under past conditions. For example, Lackmann (2015) estimated
88 the thermodynamic contribution of recent climate change to the evolution of Hurricane Sandy by comparing a control run to a
89 PGW simulation using boundary conditions that were adjusted to reflect the climate of the late 19th Century. Likewise, Kawase
90 (2008) used a similar approach in a climate change attribution study of the Mei-yu rain band in southern China. Here we use
91 the PGW method to quantify what the magnitude of surface melt would have been if the recent dynamical forcing of the ice
92 sheet had occurred in a preindustrial thermodynamic background state by answering the following questions: (1) How much
93 of the recent SMB decline can be attributed to the combined influence of increasing background temperatures and contributions

Deleted: a

Deleted: SIC and SST

Deleted: anomalies

Deleted: GrIS

Deleted: . Modeling work has provided one explanation for the lack of marine influence by demonstrating that persistent katabatic outflow over the ice sheet acts as a barrier to onshore advection (Hanna et al., 2014; Noël et al., 2014)

Deleted: sea-surface conditions

Deleted: S

Deleted: preceding GrIS melt events .

Deleted: demonstrated

Deleted: elling

Deleted: GrIS

Deleted: (Stroeve et al., 2017)

Field Code Changed

Deleted: GrIS

Deleted: sea-surface conditions

Deleted: both

Deleted:

Deleted: sea-surface conditions

Deleted: only

Deleted: GrIS

Deleted: since its acceleration around the turn of the century

Deleted: more systematic

Deleted: GrIS

Deleted: (typically some future period)

Deleted: GrIS

Deleted: setting

Deleted: . Specifically, this analysis aims to answer the

Deleted: local thermodynamic change (i.e.,

from local SSCs? (2) What portion of the thermodynamic influence is due to adjacent SSC change alone and do SSCs have a discernible impact on the timing or duration of the melt season?

2. Experimental Design

A model schematic outlining our approach is presented as Figure 1. Atmospheric conditions and the SMB and surface energy balance (SEB) response were modeled using the regional climate model, Modèle Atmosphérique Régional (MAR) (Fettweis et al., 2005, 2020; Lefebvre et al., 2005). MAR includes a surface-atmosphere energy and mass transfer scheme with a one-dimensional snowpack model that represents snow grain metamorphism and its impact on albedo, and accounts for the percolation and refreeze of meltwater within the snowpack (Amory et al., 2021; Brun et al., 1989, 1992). For a more detailed description of MAR, see Amory et al. (2021). Here, we employed MAR version 3.12 initialized and forced at its lateral boundaries with 6-hourly ERA5 reanalysis data and integrated over a 120x180, 20-km grid with 24 vertical atmospheric levels.

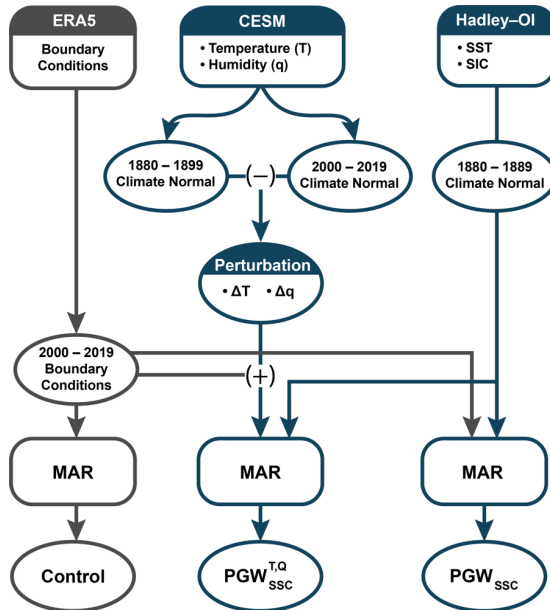


Figure 1. Model experiment overview. Model schematic illustrating the design of the control run (gray outlines) and pseudo-global warming experiments (blue outlines). For the control run, all boundary fields including SSCs were sourced from ERA5. In $PGW_{SSC}^{T,Q}$, the atmospheric thermodynamic fields of air temperature (T) and specific humidity (Q) from ERA5 were adjusted to reflect preindustrial conditions by applying a climate change perturbation signal derived from Community Earth System Model (CESM) data, and preindustrial SSCs of SST and SIC were prescribed using merged Hadley-OI observational data. In PGW_{SSC} , only SST and SIC were altered to reflect preindustrial conditions.

Deleted: sea-surface conditions)

Deleted: SIC / SST

Deleted: ? (3) Do

Deleted: sea-surface conditions

Deleted: GrIS

Deleted: GrIS

Deleted: we refer the reader to

Deleted: sea surface conditions

Deleted: sea-surface conditions (

Deleted:)

:50

:51 As a control, we forced MAR with ERA5 data spanning 2000 to 2019 to provide a representation of historical conditions
:52 during the recent period of anomalous Greenland blocking (Figure 1, gray components). For the control run, all boundary
:53 fields including the SSCs of sea-surface temperature (SST) and SIC were sourced from ERA5. To simulate the preindustrial
:54 thermodynamic state (Figure 1, blue components), we adjusted the boundary conditions of air temperature and specific
:55 humidity using perturbations obtained from the NCAR Community Earth System Model-Large Ensemble (CESM-LE) project
:56 (Kay et al., 2015), while zonal and meridional winds at the model boundaries were left unaltered to minimize differences in
:57 the large-scale atmospheric circulation between the experiment and the control. For the pre-industrial simulations, we adjusted
:58 ERA5 air temperature and specific humidity using a climate change perturbation derived from the 40 ensemble members of
:59 the NCAR CESM-LE project as follows:

:60

:61

:62

$$\Delta x = \bar{x}_p - \bar{x}_c$$

:63

:64

:65

:66

:67

:68

:69

:70

:71

:72

:73

:74

:75

:76

:77

:78

:79

:80

:81

:82

:83

Deleted: the

Deleted: period

Deleted: and the attendant acceleration of GrIS surface melt

Deleted: sea surface conditions

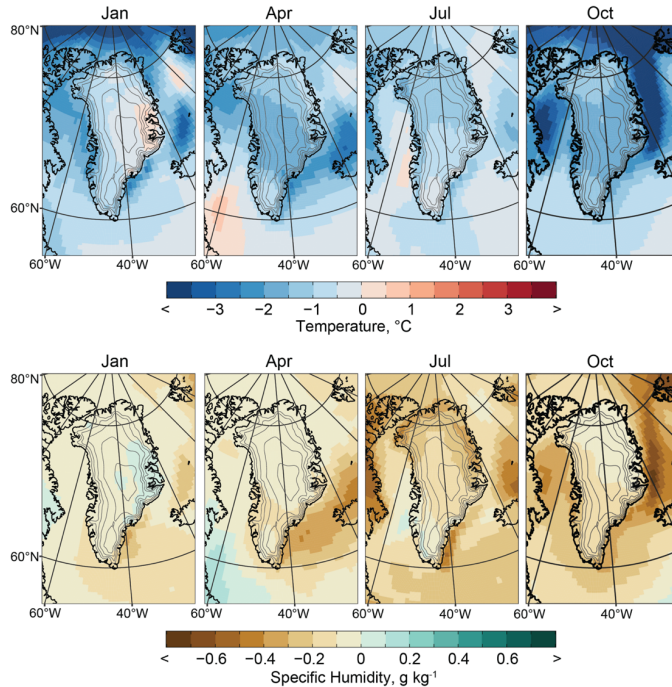
Deleted: The same is true for observations.

Deleted: GrIS

Deleted: under global warming

.91
.92
.93
.94
.95
.96

Figure 2 shows a subset of the monthly surface air temperature and specific humidity perturbation fields that were applied at the lateral boundaries of MAR. Seasonally, CESM-LE simulates the greatest temperature difference in fall and winter (Fig. 2, top row), consistent with what should be expected under Arctic amplification, which is largely driven by sea ice loss (Screen and Simmonds, 2010). Differences in near-surface atmospheric moisture are largely reflective of the Clausius-Clapeyron relation, with drier conditions mirroring locations of cooler temperatures in the preindustrial climate (Fig. 2, bottom row).



.97 **Figure 2. Climate change perturbation fields.** Perturbation fields derived from CESM-LE for surface air temperature (top row) and specific
.98 humidity (bottom row) shown for a selection of months equally spaced throughout the year as labeled at the top of each panel. Perturbation
.99 fields shown for the lowermost model level after vertically interpolating to the same ECMWF L137 hybrid sigma-pressure levels as the
.00 ERA5 boundary conditions. Contour interval: 500 m. Range: 1000–3000 m.
.01

.02 The use of a GCM-derived perturbation signal presents issues when dealing with sea ice. The change in SIC is greatest along
.03 the sharply defined sea ice front and the GCM's representation may not geographically align with observations. Figure 3
.04 presents one such comparison for June 15, 2018, which occurs during a month of exceptionally low SIC in the Greenland Sea.

Deleted: , where conditions over the surrounding seas were more than 3 °C cooler during the preindustrial period than in the current climate ...

Deleted: . The spatial distribution and seasonality of this temperature perturbation signal is

Deleted: ,

Deleted: in

Deleted: e part

Deleted: ,

Deleted: , however,

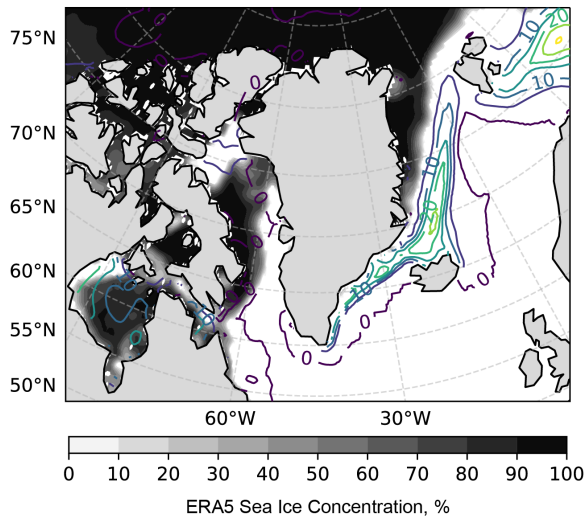
Deleted: sea ice concentration (

Deleted:)

Deleted: This misalignment is quite apparent when comparing the perturbation signal to the sub-daily observations used to force the RCM. ...

20 There is a considerable gap between the observed sea ice front and area of greatest SIC change according to CESM-LE, such
 21 that the application of this perturbation signal would result in a locally high SIC stretching from Iceland to Svalbard that is
 22 separated from the main body of sea ice. To avoid this unrealistic distribution, and to ensure consistency between SIC and
 23 SST, we prescribed both SIC and SST in our experimental simulations using 1880–1899 long-term monthly means calculated
 24 from the merged Hadley-OI observational dataset (Shea et al., 2020) and interpolated to a 6-hourly timestep.

Deleted: minimum in SIC stretching along the original sea ice front, followed by a band of higher
Deleted: circumstance
Deleted: sea-surface temperature (
Deleted:)



25 **Figure 3. Sea ice representation.** Comparison of observed sea ice concentration on June 15, 2018 (shading) and the corresponding CESM-
 26 LE climate perturbation signal (contours, 5% interval).
 27

28 Contrary to global SST trends, there are extensive areas around Greenland where SST during the preindustrial period was
 29 higher than during the current period—i.e., SST has decreased throughout much of the region since the preindustrial period
 30 (Figure S2). This is most apparent during winter and spring when higher preindustrial SST is observed throughout the northern
 31 subpolar gyre to the southeast of Greenland and extending from the southern Greenland coast along the sea ice edge to
 32 Svalbard. The spatial and seasonal pattern of lower SST since the preindustrial period matches the fingerprint of the so-called
 33 North Atlantic warming hole—an observed decrease in subpolar North Atlantic SST that has been attributed to a weakening
 34 of the Atlantic meridional overturning circulation and associated poleward oceanic heat transport as a consequence of climate
 35 change (Caesar et al., 2018). In summer, SST throughout much of the region was lower during the preindustrial period (Figure
 36 S2).

Deleted: 1
Deleted: In summer, SST throughout much of the region was lower during the preindustrial period (Figure S1).
Deleted: global

46
 47 After interpolating the Hadley-OI fields to a 6-hourly timestep, we applied the following adjustments based on the work of
 48 Hurrell *et al.* (2008) to further ensure consistency between SST and SIC:

- 49 • If an interpolated grid cell had a SIC > 90%, we set the SST of that cell to the sea ice freezing point of -1.8 °C.
- 50 • Where 15% < SIC < 90% we adjusted SST as follows:

51
$$SST = 9.328(0.729 - (SIC/100)^3) - 1.8, \quad (1)$$

- 52 • SIC was set to zero if SST > 4.97 °C.
- 53 • Where -1.8 °C < SST < 4.97 °C we adjusted SIC as follows:

54
$$SIC = 100(0.729 - (SST + 1.8)/9.328)^{\frac{1}{3}}, \quad (2)$$

55
 56 Following Noël *et al.* (2014), we allotted 5 years of spin-up time for each model simulation to allow the MAR snowpack model
 57 to adjust to the altered boundary conditions. In $PGW_{SSC}^{T,Q}$, we adjusted the boundary forcing fields of temperature (T), specific
 58 humidity (Q), and the SSCs of SST and SIC to reflect the long-term preindustrial conditions. Thus, by comparing $PGW_{SSC}^{T,Q}$ to
 59 the control simulation, we quantify the thermodynamic contribution to recent surface mass loss. For PGW_{SSC} , we adjusted SST
 60 and SIC to reflect preindustrial conditions, while leaving the temperature and humidity fields unaltered. ~~(see (1) and (2))~~ quantify the
 61 portion of recent surface mass loss that is due to changes in local SSCs.

62
 63 The design of PGW_{SSC} also allows us to test how much of the mechanism identified by Stroeve *et al.* (2017) – that low spring
 64 SIC in the seas surrounding Greenland preconditions the ice sheet for melt in early melt onset years – is due to direct
 65 thermodynamic forcing alone. Following Stroeve *et al.* (2017), we define melt onset as the first instance of five or more
 66 consecutive days of melt. The date of freeze onset is then defined as the first day following the last instance of five or more
 67 consecutive days of melt. We calculated all measures of the melt season at each MAR grid pixel, then tested for significant
 68 differences between the PGW simulations and the control using a paired Wilcoxon signed-rank test (Wilcoxon, 1945) with a
 69 predetermined significance level of $\alpha = 0.05$ (i.e., 95 % confidence level).

Deleted: The analysis presented below includes comparisons between the two PGW simulations and the control simulation (Fig. 1). ...

Deleted: PGW1

Deleted: .

Deleted: using the procedures detailed above

Deleted: PGW1

Deleted: GrIS

Deleted: PGW2

Deleted: . In doing so, we

Deleted: sea-surface conditions

Deleted: PGW2

Deleted: the theory

Deleted: of

Deleted: (2017)

Field Code Changed

Deleted: GrIS

Deleted: (2017)

Field Code Changed

Deleted: and melt season length as the number of days spanning the two dates...

89 **3. Results**

90 **3.1. Thermodynamic Contribution to SMB Change**

91 Figure 4 presents a comparison of the cumulative SMB anomaly between the control run and each PGW simulation. The
 92 control run (Fig. 4, gray line) shows a cumulative SMB anomaly of -1852 Gt over the study period of 2000 to 2019, congruent
 93 with other estimates (IMBIE, 2020). This decline in the SMB corresponds to approximately 5 mm of global sea level rise. A
 94 gradual shift to a negative cumulative SMB occurs around 2005, coinciding with the transition to a more persistently negative
 95 NAO and rise in Greenland blocking frequency (Hanna et al., 2015; Hofer et al., 2017). The first instance of pronounced mass
 96 loss is evident as a sharp decrease in 2007—a year of unprecedented surface melt up to that point in the satellite record (Mote,
 97 2007). The exceptional melt years of 2012 (Hanna et al., 2014; Nghiem et al., 2012) and 2019 (Cullather et al., 2020; Hanna
 98 et al., 2021; Tedesco and Fettweis, 2020) are readily apparent as drops in the control time series. We examine these two years
 99 in more detail in section 3.4.



00 **Figure 4. Temporal evolution of the SMB under contrasting thermodynamic background conditions.** Shown are the cumulative SMB
 01 anomaly time series for the control (gray), $PGW_{SSC}^{T,Q}$ (blue dashed), and PGW_{SSC} (green dashed) simulations. Anomalies calculated with
 02 respect to the 1980-1989 reference period. Left axis shows cumulative SMB anomaly; right axis shows the equivalent sea-level contribution.
 03 Annotations detail the difference in the final cumulative SMB between each of the PGW simulations and the control.
 04

05 Comparing the control with $PGW_{SSC}^{T,Q}$ (Fig. 4, blue dashed line) highlights the substantial thermodynamic contribution to the
 06 recent change in SMB. A difference in cumulative SMB between the two simulations of 1145 Gt amounts to a 62% reduction
 07 in surface mass loss in $PGW_{SSC}^{T,Q}$ relative to the control. Under the preindustrial thermodynamic setting of $PGW_{SSC}^{T,Q}$, the ice sheet
 08 maintains a positive SMB anomaly through 2009, and the mass loss for each melt season is much more subdued relative to the
 09 control. This holds true for the exceptional melt years of 2012 and 2019; however, while the magnitude of mass loss is greater
 10 when the warming signal is included, the relative contribution of those individual melt seasons to the total SMB change over
 11 the 20-year period is greater for $PGW_{SSC}^{T,Q}$.—In a preindustrial climate, 2012 and 2019 each account for ~250 Gt of mass loss,

Deleted: GrIS

Deleted: of the

Deleted: s

Deleted: Instances of marked mass loss are frequently evident in the years that follow; however, t

Field Code Changed

Deleted: precipitous

Deleted: exceptional melt

Deleted: GrIS

Deleted: PGW1

Formatted: Font: 10 pt

Formatted: Font: 10 pt

Formatted: Font: 10 pt

Deleted: PGW2

Formatted: Font: 10 pt

Formatted: Font: 10 pt

Deleted: PGW1

Deleted: clearly

Deleted: GrIS

Deleted: PGW1

Deleted: PGW1

Deleted: GrIS

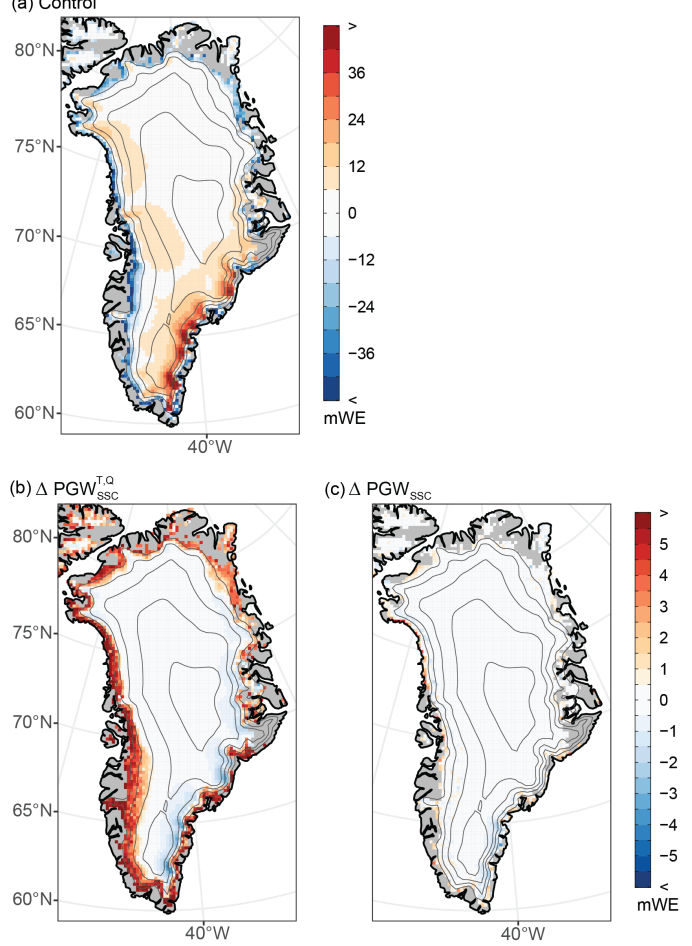
Deleted: while the dynamical forcing of the ice sheet is still evident in the negative anomalies that occur during individual summers, ...

Deleted: anthropogenic

Deleted: PGW1

.33 which – combined – is approximately 2/3 of the total mass loss in $PGW_{SSC}^{T,Q}$ (Fig. 4). Furthermore, while the rate of mass loss
 .34 is reduced from 2013 to 2018 in the control, this period undergoes a slight surface mass gain in $PGW_{SSC}^{T,Q}$.

Deleted: PGW1
 Deleted: much
 Deleted: PGW1



.35 **Figure 5. Spatial distribution of SMB change under contrasting thermodynamic background conditions.** (a) The cumulative SMB
 .36 anomaly over the full study period of 2000–2019 as represented by the control simulation. (b) $PGW_{SSC}^{T,Q}$ cumulative SMB minus the control.
 .37 (c) PGW_{SSC} cumulative SMB minus the control. Contour interval: 500 m. Range: 1000–3000 m.

Deleted: GrIS
 Deleted: PGW1
 Formatted: Font: 10 pt
 Formatted: Font: 10 pt
 Formatted: Font: 10 pt
 Deleted: PGW2
 Formatted: Font: 10 pt
 Formatted: Font: 10 pt

44

45 The cumulative SMB anomaly in PGW_{SSC} (Fig. 4, green dashed line) is 105 Gt greater than that for the control. This relatively
46 small difference indicates that there has been minimal direct influence by changes in local SST and SIC over the study period—
47 a result that is consistent with previous modeling studies which showed low SMB sensitivity when applying arbitrary
48 perturbations to local SSCs (Hanna et al., 2009, 2014; Noël et al., 2014). This agreement across varying methodological
49 approaches adds confidence that changes occurring more widely throughout the Arctic and sub-Arctic dominate the
50 thermodynamic contribution to mass loss.

Deleted: PGW2

Deleted: GrIS

Deleted: sea-surface conditions

Deleted: GrIS

51
52 The cumulative SMB over the study period in the control (Fig 5a) shows a band of negative SMB along the perimeter of the
53 ice sheet that clearly demarcates the ablation zone. The greatest accumulation occurs along the southeast coast of Greenland
54 and is a product of orographic enhancement of precipitation associated with lee-side cyclones that form in westerly flow over
55 southern Greenland (Bromwich et al., 1998; Rogers et al., 2004; Schuenemann et al., 2009). Other areas of notable SMB gains
56 include west and northwest Greenland. Snow accumulation in these areas is fueled by bouts of intense water vapor transport
57 through the Davis Strait that have increased in frequency in recent decades (Mattingly et al., 2016, 2018).

Deleted: Figure 5 provides a spatial representation of the comparisons made in Fig. 4. The map

Deleted: of

Deleted: as modeled by

Deleted: , where annual surface mass loss exceeds accumulation

58
59 Relative to the control, $PGW_{SSC}^{T,Q}$ yields a greater cumulative SMB in a band that stretches around the perimeter of the ice sheet,
60 exceeding 2000 m elevation in some locations in southwest Greenland (Fig 5b). This positive anomaly with respect to the
61 control is a consequence of decreased meltwater runoff in the preindustrial setting (Fig. S3a). At higher elevations over much
62 of eastern Greenland and to a lesser extent over the northwest ice sheet, a reduction in snowfall in the cooler and dryer
63 atmosphere of $PGW_{SSC}^{T,Q}$ results in a lower SMB compared to the control (Fig 5b, Fig. S3b). This represents a competing
64 influence on SMB, as the same bouts of remotely sourced heat and moisture that promote melt at lower elevations can also
65 deliver anomalous snow accumulation over high elevations, thereby offsetting SMB losses directly, through increased mass
66 gains, and indirectly, by increasing the surface albedo (Bailey and Hubbard, 2025; Mattingly et al., 2018).

Deleted: PGW1

Deleted: Supplementary

Deleted: 2

Deleted: PGW1

Deleted: Supplementary

Deleted: 2

67
68 The greatest differences in surface runoff between $PGW_{SSC}^{T,Q}$ and the control are centered on mid-to-late July (Fig. 6a). The
69 gray shading in Fig. 6 depicts the 1 std. dev. range about the mean that was simulated for each variable across the 20-year
70 control run, revealing that runoff during the peak of the melt season in $PGW_{SSC}^{T,Q}$ was nearly 1 std. dev. below what has been
71 typical since the turn of the century. The relative mass loss over high elevations evident in Fig 5b is driven by a reduction in
72 snowfall throughout the cool season; however this impact on snow accumulation is most apparent in fall and early winter when
73 the greatest change in background conditions have occurred (Fig. 2, 7b) (Serreze and Barry, 2011). In contrast with the rest of
74 the year, there is a slight increase in summer snowfall in $PGW_{SSC}^{T,Q}$ that coincides with a reduction in rainfall (Fig. 6c),
75 consistent with the historical record which shows greater partitioning toward liquid precipitation as the atmosphere has warmed
76 in recent decades (Box et al., 2023; van den Broeke et al., 2016).

Deleted: Figure 6 shows the average seasonal progression of the principal SMB components for each model simulation.

Deleted: PGW1

Deleted: the peak of the melt season in

Deleted: to provide context regarding magnitude of the differences between the experiment and the control. This

Deleted: s

Deleted: PGW1

Deleted: under Arctic amplification

Deleted: PGW1

Deleted: frozen

Deleted: under the cooler preindustrial setting

04

05 The differences between PGW_{SSC} and the control show a similar pattern as observed for $PGW_{SSC}^{T,Q}$, however, they are
06 comparatively minimal in both magnitude and scale (Fig 5c). The change in $SSCs$ reduces meltwater runoff resulting
07 in higher SMB (Fig 5c, Fig. S3d). Unlike $PGW_{SSC}^{T,Q}$, this response is largely confined to grid cells along the periphery of the ice
08 sheet. The isolated impact of $SSCs$ on snowfall is most evident along the southeast margin of the ice sheet and above ~1000
09 m in northwest Greenland. Whereas runoff was diminished throughout the entire melt season $PGW_{SSC}^{T,Q}$, the impact of $SSCs$
10 alone on surface melt emerges later (Fig. 6a), likely reflecting the stronger coupling between ocean and atmosphere as the
11 thermal gradient between them increases into the fall (Screen, 2017).

Deleted: PGW2

Deleted: PGW1

Deleted: sea-surface conditions

Deleted: in

Deleted: PGW_{SSC}

Deleted: PGW2

Deleted:

Deleted: Supplementary

Deleted: 1

Deleted: PGW1

Deleted: terminus

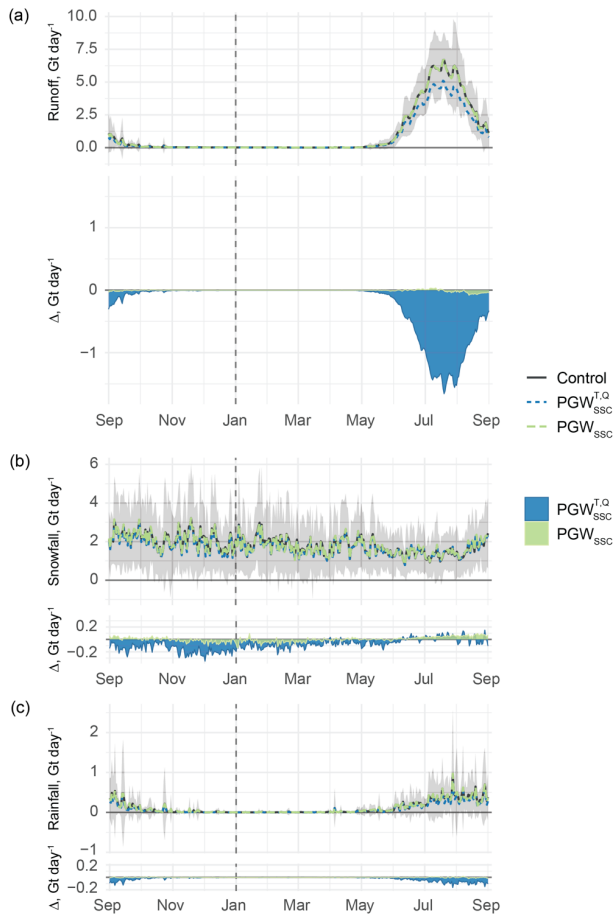
Deleted: sea-surface conditions

Deleted: In contrast with PGW1,

Deleted: in which

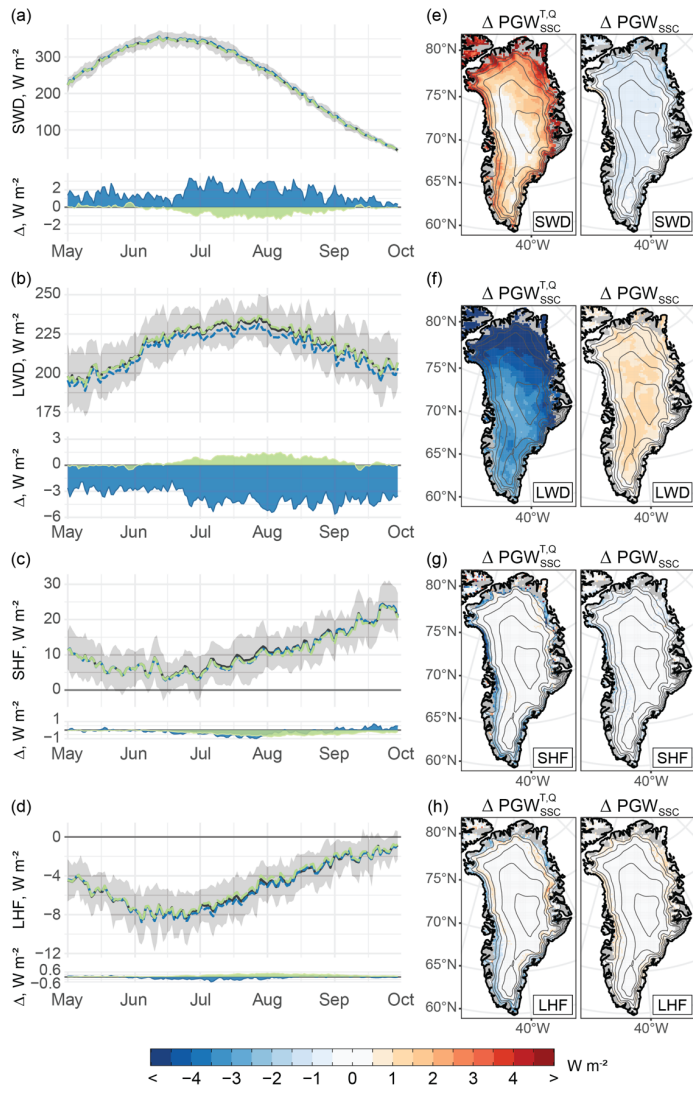
Deleted: sea-surface conditions

Deleted: in the melt season



28 **Figure 6. Seasonal evolution of the SMB under contrasting thermodynamic background conditions.** Panels depict the seasonal
 29 progression of three principal SEB components: (a) Surface runoff, (b) snowfall, (c) rainfall. Top portion of each panel shows 2000–2019
 30 long-term daily mean totals of each SMB component throughout the melt season for the control (gray), $PGW_{ssc}^{T,Q}$ (blue dashed), and PGW_{ssc}
 31 (green dashed) simulations. Time series represent the spatially integrated sum of a given variable over the entire ice mask. Gray shading
 32 shows the 1σ range about the mean for the control simulation. Bottom portion shows the difference between each PGW simulation ($PGW_{ssc}^{T,Q}$
 33 blue; PGW_{ssc} green) and the control ($\Delta = PGW - \text{Control}$). The scale of the y-axis on the bottom portion is kept constant across all panels
 34 to facilitate comparison between SMB terms.

- Deleted: GrIS
- Deleted: PGW1
- Deleted: PGW2
- Formatted: Font: 10 pt
- Formatted: Font: 10 pt
- Formatted: Font: 10 pt
- Formatted: Font: 10 pt
- Formatted: Font: 10 pt
- Formatted: Font: 10 pt
- Deleted: PGW1
- Formatted: Font: 10 pt
- Formatted: Font: 10 pt
- Formatted: Font: 10 pt
- Deleted: PGW2
- Formatted: Font: 10 pt
- Formatted: Font: 10 pt



41 **Figure 7. The SEB of the Greenland Ice Sheet during the melt season under contrasting thermodynamic background conditions.** (a–
 42 d) Top portion of each panel shows the 2000–2019 long-term daily mean values of each SEB component throughout the melt season for the
 43 control (gray), $PGW_{SSC}^{T,Q}$ (blue dashed), and PGW_{SSC} (green dashed) simulations. Time series represent the spatial average taken over the
 44 entire ice mask for a given variable. Gray shading shows the 1 σ range about the mean for the control simulation. Bottom portion shows the
 45 difference between each PGW simulation ($PGW_{SSC}^{T,Q}$, blue; PGW_{SSC} , green) and the control ($\Delta = PGW - Control$). The scale of the y-axis on
 46 the bottom portion is kept constant across all panels to facilitate comparison between SEB terms. (e–f) Maps depicting the difference between
 47 the 2000–2019, Jun–Aug long-term mean of each SEB component between each PGW simulations ($PGW_{SSC}^{T,Q}$, left; PGW_{SSC} , right) and the
 48 control. SEB components are organized by row: (a, e) downward shortwave radiation (SWD); (b, f) downward longwave radiation (LWD);
 49 (c, g) sensible heat flux (SHF); (d, h) latent heat flux (LHF). Contour interval: 500 m. Range: 1000–3000 m.
 50

51 While a decrease in snowfall relative to the control in the PGW simulations partially compensates for the relative mass gains
 52 at lower elevations, the reduction in meltwater runoff is the primary determinant of the differences in cumulative SMB
 53 observed in Fig. 4. Recognizing this, the next section focuses on the extended melt season to better understand the mechanisms
 54 by which thermodynamic change has dictated surface runoff.

55 3.2. Thermodynamic Drivers of Surface Runoff

56 The preindustrial thermodynamic state of $PGW_{SSC}^{T,Q}$ is associated with an increase in downward shortwave radiation (SWD)
 57 (Fig. 7a, e) and a decrease in downward longwave radiation (LWD) (Fig. 7b, f) throughout the melt season. For both variables,
 58 the differences between the control and $PGW_{SSC}^{T,Q}$ are greatest over the northern ice sheet. This is consistent with the
 59 thermodynamic signature in the free atmosphere where the differences in both temperature and specific humidity at 600 hPa
 60 are maximized over northern Greenland (Fig. S4). Turbulent fluxes are generally diminished in $PGW_{SSC}^{T,Q}$ relative to the control
 61 (Fig. 7c,d). Differences in the turbulent heat fluxes are focused along the outer margins of the ice sheet, where lower elevations
 62 display a decrease in both sensible (SHF) and latent heat flux (LHF) in $PGW_{SSC}^{T,Q}$ that is mirrored by differences of the opposite
 63 sign over higher elevations (Fig. 7g, h).
 64

65 The juxtaposition in the response of the turbulent fluxes in $PGW_{SSC}^{T,Q}$ appears to arise from opposing direct and indirect responses
 66 to the change in background conditions. Along the ice sheet margins, a decrease in both SHF and LHF is consistent with a
 67 direct reduction in the flux of heat and moisture to the surface of the ice sheet in a colder, drier preindustrial atmosphere.
 68 Conversely, above normal turbulent fluxes over higher elevations follow indirectly from changes in the near-surface wind
 69 field. Lower water vapor content in $PGW_{SSC}^{T,Q}$ (Fig. 2) reduces the longwave emissivity of the atmosphere, which would act to
 70 lower surface temperatures, increase the near-surface potential temperature deficit, and thereby strengthen the katabatic winds
 71 over the upper portion of the steep margins of the ice sheet (Fig. 8b) (van den Broeke et al., 2009b; Gortler et al., 2014). Stronger
 72 katabatic winds then increase turbulent heat flux by mixing relatively warm air through the stable boundary layer to the surface
 73 (Fig. 7g, h).
 74

- Deleted: GrIS
- Deleted: PGW1
- Deleted: PGW2
- Formatted ... [1]
- Formatted ... [2]
- Deleted: PGW1
- Deleted: PGW2
- Formatted ... [3]
- Formatted ... [4]
- Deleted: May
- Deleted: Sep
- Deleted: PGW1
- Deleted: PGW2
- Formatted ... [5]
- Formatted ... [6]
- Deleted: it is clear that
- Deleted: Thus, the influence of recent thermodynamic change on GrIS SMB has been consequential during the melt season.
- Deleted: GrIS
- Deleted: GrIS
- Deleted: Figure 7 contrasts the SEB of the GrIS between the control and PGW simulations.
- Deleted: PGW1
- Deleted: PGW1
- Deleted: 3
- Deleted: The time series in Fig. 7c and d indicate that the t
- Deleted: PGW1
- Deleted: The magnitude of these differences is far less than what is observed for the radiative terms; however, this is partly attributable to a spatially heterogeneous response.
- Deleted: PGW1
- Deleted: PGW1
- Deleted: s
- Deleted: . Figure 8a shows the long-term mean
- Deleted: Jun
- Deleted: May–
- Deleted: Aug
- Deleted: Sep 10 m winds for the control period, clearly illustrating the persistent katabatic wind signature over Greenland
- Deleted: PGW1
- Deleted: GrIS

While the differences in the radiative terms considerably outweigh that of the turbulent fluxes in $PGW_{SSC}^{T,Q}$, this is not the case for PGW_{SSC} . Although the minor differences in SWD and LWD are more widespread (Fig. 7e, f), the magnitude of the impact of SSC_s on turbulent heat flux is greater in some locations along the ice sheet margins, particularly as is evident in the reduction in SHF along the northern and central portions of the western ablation zone (Fig. 7g). This appears to be primarily a consequence of the indirect katabatic wind adjustment. The lower SST and higher SIC in PGW_{SSC} reduces the horizontal temperature gradient between the ice sheet and surrounding seas which, as has been documented in previous work (Noël et al., 2014), causes a weakening of the katabatic wind along the ice sheet margins (Fig. 8c)—a change that would reduce turbulent mixing, and thus SHF, to the surface, while also causing a reduction in evaporation / sublimation and increasing LHF relative to the control.

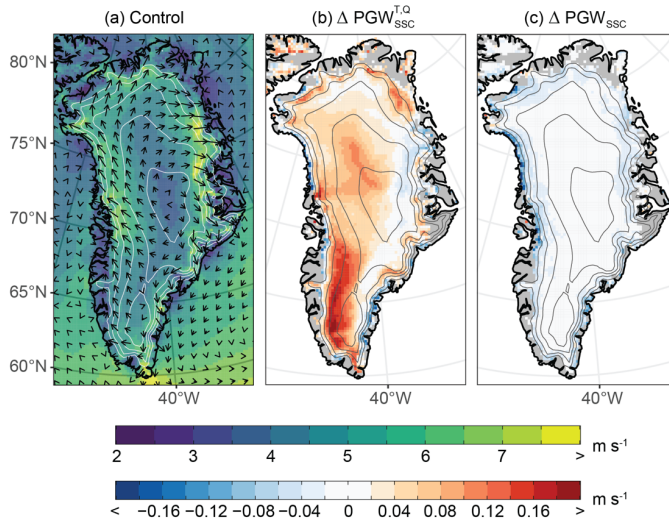


Figure 8: Melt season katabatic wind field under contrasting thermodynamic background conditions. (a) 2000–2019 long-term mean Jun–Aug 10 m wind speed (shading) and direction (vectors). (b) Difference in 10 m wind speed between $PGW_{SSC}^{T,Q}$ and the control. (c) Difference in the 10 m wind speed between PGW_{SSC} and the control. $\Delta = PGW - \text{Control}$. Contour interval: 500 m. Range: 1000–3000 m.

The consistent and widespread reduction in LWD in $PGW_{SSC}^{T,Q}$ (Fig. 7b and f) is not surprising given the drier atmospheric conditions that prevailed during the preindustrial period. The spatial distribution of integrated water vapor (IWV) anomalies with respect to the control closely resemble that for LWD (c.f. Fig. 9e and 7f). Note that the LWD anomalies in Fig. 7b and f do not provide a complete picture of the impact on the SEB, as any resulting change in the temperature of the ice sheet's surface would be offset to some degree by a change in emitted longwave radiation in accordance with the Planck feedback.

Deleted: PGW1

Deleted: PGW2

Deleted: sea-surface conditions

Deleted: PGW2

Deleted: ,

Deleted: . The decrease in the near-surface wind field

Deleted:

Deleted: which

Deleted: , resulting in an increase in

Deleted: May

Deleted: Sep

Deleted: PGW1

Formatted: Font: 10 pt

Formatted: Font: 10 pt

Formatted: Font: 10 pt

Deleted: PGW2

Formatted: Font: 10 pt

Formatted: Font: 10 pt

Formatted: Font: (Default) +Body (Times New Roman), English (US)

Formatted: Font: (Default) +Body (Times New Roman), English (US)

Deleted: that is visible for

Deleted: PGW1

Deleted: The specific humidity perturbation signal that was applied to...

Deleted: PGW1

Deleted: (see Fig. 2)

Deleted: is manifest in the integrated water vapor (IWV) over the ice sheet (Fig. 9a, e).

Deleted: the

Deleted: —highlighting the effectiveness of water vapor as a greenhouse gas and nicely illustrating the cause of the longwave radiative response

Deleted: It is important to note that t

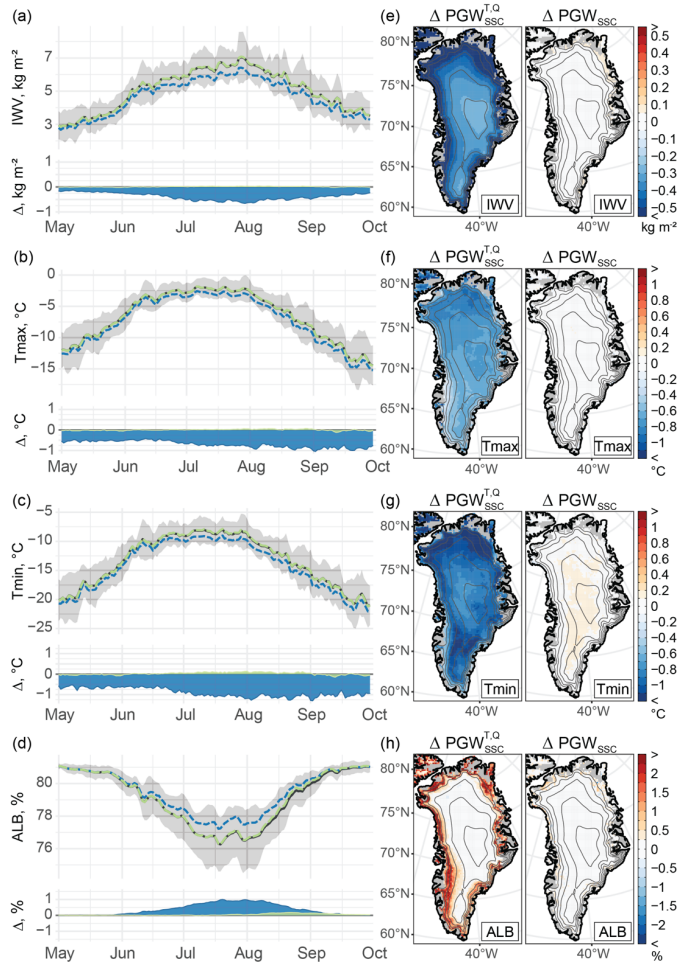
Deleted: end

.90 Indeed, this can be seen in Fig. S5, which depicts a weaker and less uniform response across the ice sheet when considering
.91 the difference in net longwave radiation between $PGW_{SSC}^{T,Q}$ and the control; however, it remains the case that the preindustrial
.92 setting of $PGW_{SSC}^{T,Q}$ produces reductions in net longwave radiation that are most evident over northern Greenland.

.94 The consequence of this water vapor feedback can be seen in the ice-sheet-wide drop in surface temperature in $PGW_{SSC}^{T,Q}$. The
.95 magnitude of the Tmax and Tmin anomalies in $PGW_{SSC}^{T,Q}$ both increase from spring into fall (Fig. 9b, c). This seasonal pattern
.96 is consistent with stronger Arctic amplification in the fall than in spring as pan-Arctic reductions in SIC in a warmer climate
.97 allow for increased heat flux from the ocean to the comparatively cool fall atmosphere (Chung et al., 2021). Additionally, there
.98 is a decline in downward shortwave radiation as the solar declination decreases into winter, which elevates the relative
.99 contribution of longwave radiative effects to the SEB (Lenaerts et al., 2019; Wang et al., 2018, 2019). There is a distinct north-
.00 south gradient in the maximum daily surface air temperature (Tmax) response (Fig. 9f). The weaker Tmax differences over
.01 southern Greenland in $PGW_{SSC}^{T,Q}$ are a consequence of both a higher sun angle at lower latitudes and the lower surface albedo
.02 of the southern ice sheet, both of which decrease the relative longwave contribution to the SEB. At night, LWD constitutes the
.03 sole radiative input to the SEB. Consequently, the Tmin response is notably greater than Tmax and it more closely resembles
.04 that of IWV (Fig. 9e) and LWD (Fig. 7f).

.06 $PGW_{SSC}^{T,Q}$ exhibits a band of higher surface albedo throughout the melt season that runs along the perimeter of the ice sheet (Fig.
.07 9d, h) and closely aligns with areas where IWV (Fig. 9e), Tmin, (Fig. 9g), SHF (Fig. 7g), and surface runoff (Fig. S3a) are
.08 reduced, relative to the control. Thus, the longwave radiative response to reduced water vapor content combined with
.09 diminished SHF in a cooler atmosphere appear to be critical factors contributing to lower surface runoff under the preindustrial
.10 background conditions of $PGW_{SSC}^{T,Q}$. The reduction in water vapor decreases LWD, which allows for lower Tmin. These changes
.11 would reduce runoff directly, by increasing the portion of meltwater that is refrozen within the snowpack, and indirectly, by
.12 diminishing the ice-albedo feedback. The interdependence between SEB components is effectively illustrated by the
.13 differences in net shortwave radiation between $PGW_{SSC}^{T,Q}$ and the control (Fig. S5)—the magnitude of the differences in net
.14 shortwave radiation exceeds that for SWD along the perimeter of the ice sheet, emphasizing the importance of the ice albedo
.15 feedback. That the strongest signal is located over the northern Greenland and aligned with some of the largest increases in
.16 surface albedo supports previous work demonstrating the importance of this longwave radiative mechanism to runoff from
.17 northern Greenland (Noël et al., 2014).

- Deleted: 4
- Deleted: PGW1
- Deleted: PGW1
- Deleted: the
- Deleted: GrIS
- Deleted: simulated by
- Deleted: PGW1
- Deleted: Here, the differences in the seasonality, magnitude, and spatial distribution of the maximum (Tmax) and minimum (Tmin) daily temperature response reflects seasonal and diurnal variations in the relative importance of longwave radiative effects, as well (... [7])
- Deleted: .
- Deleted: PGW1
- Deleted: relative to the control
- Deleted: .
- Deleted: and thus a greater water vapor feedback,
- Deleted: incoming
- Deleted: PGW1
- Deleted: The impact of surface albedo is particularly evident (... [8])
- Deleted: PGW1
- Deleted: GrIS
- Deleted: Supplementary
- Deleted: 1
- Deleted: in
- Deleted: $PGW_{SSC}^{T,Q}$
- Deleted: PGW1
- Deleted: .
- Deleted: setting
- Deleted: PGW1
- Deleted: , thereby impacting the shortwave components of (... [9])
- Deleted: PGW1
- Deleted: 4
- Deleted: clearly
- Deleted: to the thermodynamic contribution to GrIS surfic (... [10])
- Deleted: in these variables
- Deleted: the
- Deleted: GrIS
- Deleted: (Neff et al., 2014)
- Formatted: Font: 10 pt
- Field Code Changed



'68

'69 **Figure 9. Thermodynamic mechanisms of SMB change.** (a–d) Top portion of each panel shows the 2000–2019 long-term daily mean
 '70 values of each variable throughout the melt season for the control (gray), PW_{SSC}^{TQ} (blue dashed), and PW_{SSC} (green dashed) simulations.
 '71 Gray shading shows the 1σ range about the mean for the control simulation. Time series represent the spatial average taken over the entire

Deleted: GrIS

Deleted: PGW1

Deleted: PGW2

Formatted: Font: 10 pt

Formatted: Font: 10 pt

Formatted: Font: 10 pt

Formatted: Font: 10 pt

Formatted: Font: 10 pt

75 ice mask for a given variable. Bottom portion shows the difference between each PGW simulation ($PGW_{SSC}^{T,Q}$ blue; PGW_{SSC} green) and
 76 the control ($\Delta = PGW - \text{Control}$). (e–f) Maps depicting the difference between the 2000–2019, Jun–Aug, long-term mean of each variable
 77 between the PGW simulations ($PGW_{SSC}^{T,Q}$ left; PGW_{SSC} right) and the control. Variables are organized by row: (a, e) integrated water
 78 vapor (IWV); (b, f) daily maximum surface air temperature (Tmax); (c, g) daily minimum surface air temperature (Tmin); (d, h) surface
 79 albedo (ALB). Contour interval: 500 m. Range: 1000–3000 m.
 80

81 Focusing on PGW_{SSC} , it is evident that $SSCs$ alone exert minimal influence on the ice sheet. There is no clear pattern of
 82 influence on IWV or near surface air temperature (Fig. 9e–g), and an examination of temperature and humidity at 600 hPa
 83 shows no evidence of any appreciable influence on these variables in the free atmosphere (Fig. S4). There is, however, an
 84 increase in surface albedo along the western and northern margins of the ice sheet in PGW_{SSC} relative to the control that occurs
 85 late in the melt season (Fig. 9d, h) and appears to be the product of the collocated reduction in SHF (Fig. 7g).

86 3.3. Thermodynamic Change and Melt Timing

88 Consistent with previous studies (Hanna et al., 2009, 2014; Noël et al., 2014), the above results suggest that direct local marine
 89 influence on melt is limited to the outermost margins of the ice sheet. Furthermore, these results demonstrate that the influence
 90 of local sea-surface conditions is an order of magnitude less than what is observed for the full thermodynamic forcing of
 91 $PGW_{SSC}^{T,Q}$ (Fig. 4). To examine whether local SSC change may impact melt timing, Fig. 10 presents the results of a paired,
 92 signed-rank test comparing differences in median melt and freeze onset between the control and each of the PGW simulations.
 93 At lower elevations, melt onset during the 2000–2019 study period typically occurs between early-May and mid-June (Fig.
 94 10a) while freeze onset occurs from early-August through September (Fig. 10b). Later melt onset and earlier freeze onset is
 95 evident over higher elevations; however, melt in these regions is typically short-lived (Fig. 10c) and infrequent. Accordingly,
 96 the comparisons of melt timing are limited to lower elevation locations with a sufficient sample of years with melt.

98 Relative to the control, the median date of melt onset in $PGW_{SSC}^{T,Q}$ occurs, on average, ~2.5 days later, while grid cells with
 99 differences in the upper quartile showed delays in median melt onset of ≥ 4 days (Fig. 10d). Meanwhile, the median date of
 100 freeze onset advanced, by ~3.7 days on average and freeze onset in the upper quartile of grid cells shifted to ≥ 5.5 days earlier
 101 (Fig. 10e). Combined, these changes shortened the median melt season duration by an average of ~6.7 days, while melt duration
 102 in the upper quartile of grid cells shortened by ≥ 9 days. For all melt timing metrics, the differences between the $PGW_{SSC}^{T,Q}$ and
 103 the control that were deemed statistically significant at the 95% confidence level are widespread across the examined grid cells
 104 (Fig. 10d-f). In contrast, differences between PGW_{SSC} and the control exhibit a weak and inconsistent signal for all melt timing
 105 m
 106
 107
 108
 109
 110
 111
 112
 113

- Deleted: PGW1
- Deleted: PGW2
- Formatted ... [11]
- Formatted ... [12]
- Deleted: May
- Deleted: Sep
- Deleted: PGW1
- Deleted: PGW2
- Formatted ... [13]
- Formatted ... [14]
- Deleted: PGW2
- Deleted: sea-surface conditions... alone exert minimal influence on the ice sheet. There is no clear pattern of influence on IWV or near surface air temperature (Fig. 9e–g), and an examination of temperature and humidity at 600 hPa shows no evidence of any appreciable influence on these variables in the free atmosphere (Fig. S43... [15]
- Deleted: PGW2
- Deleted: GrIS
- Deleted: ¶
- Deleted: this hypothesis more directly
- Deleted: GrIS
- Deleted: timing
- Deleted: where melt occurs consistently on an interannual basis,
- Deleted: , and as mentioned in the experimental design... the comparisons of melt timing between the PGW simulations and the control ... [16]
- Deleted: experiencing
- Deleted: PGW1
- Deleted: across those regions of the
- Deleted: ice sheet
- Deleted: GrIS
- Deleted: that consistently
- Deleted: incur
- Deleted: experience
- Deleted: melt... while grid cells with differences in the upper quartile, grid cells [17]
- Deleted: experienced
- Deleted: The thermodynamic impact on the close of the m... [18]
- Deleted: on average,
- Deleted: in the fall
- Deleted: PGW1
- Deleted: PGW2

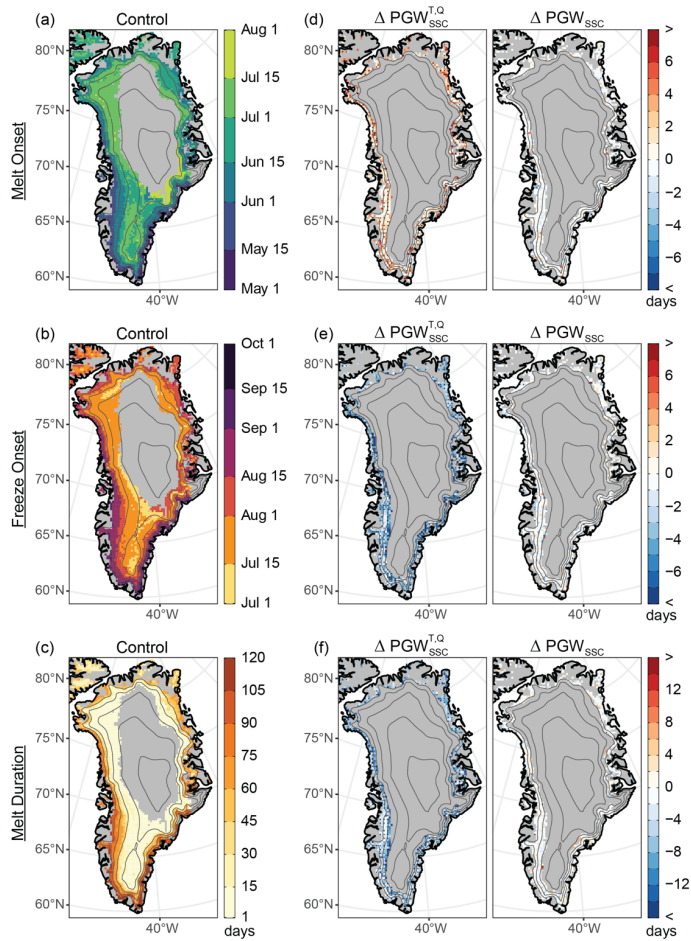


Figure 10. The impact of thermodynamic change on melt timing. The observed median date of (a) melt onset, (b) freeze onset and (c) median melt season duration for the control simulation alongside (d-f) the difference between the PGW simulations ($PGW_{SSC}^{T,Q}$ left; PGW_{SSC} right) and the control ($\Delta = PGW - \text{Control}$) for each metric as organized by row and labeled on the left. Stippling indicates differences that are statistically significant at the 95% confidence level. Contour interval: 500 m. Range: 1000–3000 m.

- Deleted: GrIS
- Deleted: PGW1
- Formatted: Font: 10 pt
- Formatted: Font: 10 pt
- Formatted: Font: 10 pt
- Deleted: PGW2
- Formatted: Font: 10 pt
- Formatted: Font: 10 pt

99 **3.4. The Exceptional Melt Years of 2012 and 2019**

00 Embedded in the long-term SMB decline (Fig. 4), 2012 and 2019 stand out as exceptional years of surface mass loss. According
01 to the control simulation, there was a cumulative SMB anomaly of -364 Gt during the 2011–2012 hydrological year (Fig. 11a).
02 The melt season of 2012 was characterized by recurrent episodes of intense surface runoff (Fig. 11b), spurred by anomalous
03 atmospheric forcing of the ice sheet (Hanna et al., 2014). Pronounced atmospheric ridging over Greenland promoted southerly
04 advection of warm, moist air to the western ice sheet (Hermann et al., 2020; Neff et al., 2014), generating strong turbulent heat
05 fluxes that drove high-volume meltwater production over the western ablation zone (Cullather et al., 2020; Fausto et al.,
06 2016b). Adiabatic cooling of remotely-sourced moist air that ascended the western slope of the ice sheet on July 12 prompted
07 the formation of low-level, liquid clouds that supplied the requisite longwave radiative forcing for widespread melt over high
08 elevations (Bennartz et al., 2013; Neff et al., 2014), generating a single day melt extent that covered over 98% of the ice sheet's
09 surface (Nghiem et al., 2012).

11 The cumulative SMB anomaly over the 2018–2019 hydrological year totaled -376 Gt (Fig. 11e). The melt season of 2019 was
12 heavily influenced by a blocking anticyclone, with origins in the European heatwave of the same year (Cullather et al., 2020;
13 Hanna et al., 2021), that produced tremendous surface runoff during a melt event centered around July 31 (Fig. 11f). The air
14 mass, which was transported west from Europe, was warmer and drier in comparison with that which was responsible for the
15 mid-July, 2012 melt event and, consequently, did not produce the same low-level cloud cover that was instrumental to melt of
16 the accumulation zone in 2012 (Tedesco and Fettweis, 2020). Consequently, while the total surface mass loss in 2019 was
17 comparable to that of 2012, observed melt was not as extensive in 2019, reaching a maximum coverage of ~73% of the ice
18 sheet's surface on July 31 (Tedesco and Fettweis, 2020).

20 For both years, the portion of observed surface mass loss that is attributable to changes in the local background thermodynamic
21 environment was less than the average for the study period: whereas the anomalous mass loss over the entire 2000–2019 study
22 period was ~62% less in $PGW_{SSC}^{T,Q}$ relative to the control, the reduction in mass loss was a relatively modest 30% and 25% in
23 2012 and 2019, respectively (Fig. 11a, e). This suggests that the record melt observed during those two summers is more a
24 consequence of exceptional atmospheric circulation patterns than it is a direct consequence of the long-term warming trend;
25 however, these exceptional circulation patterns and the long-term temperature trend may not be independent, as some studies
26 have suggested more persistent circulation regimes under global warming (Coumou et al., 2018; Overland et al., 2012; Preece
27 et al., 2023b; Screen, 2013). Indeed, this disparity is also evident over synoptic timescales—the periods of strong dynamical
28 forcing, marked by the red, vertical bars in Fig. 11, correspond to local minima in the differences in daily-mean near-surface
29 air temperature between $PGW_{SSC}^{T,Q}$ and the control. The production of meltwater and consequent surface runoff during high-
30 volume melt events is largely driven by turbulent heat fluxes (Box et al., 2022; Fausto et al., 2016b, a). It follows that the
31 longwave radiative effects of the water vapor feedback that are dictated by changes in the thermodynamic environment assume

Deleted: GrIS

Deleted: Fig. 10

Deleted: Fig. 10

Deleted: During this stretch of melt events, p

Deleted: from low latitudes

Deleted: GrIS

Deleted: Fig. 10

Deleted: Fig. 10

Deleted: GrIS

Deleted: far l

Deleted: total

Deleted: PGW1

Deleted: Fig. 10

Deleted: the relative importance of a changing background state under global climate change may be minimized during periods of strong synoptic-scale atmospheric forcing. In other words,

Deleted: it is important to note that

Deleted: (Coumou et al., 2018; Overland et al., 2012; Preece et al., 2023b; Screen, 2013)

Deleted: of the GrIS

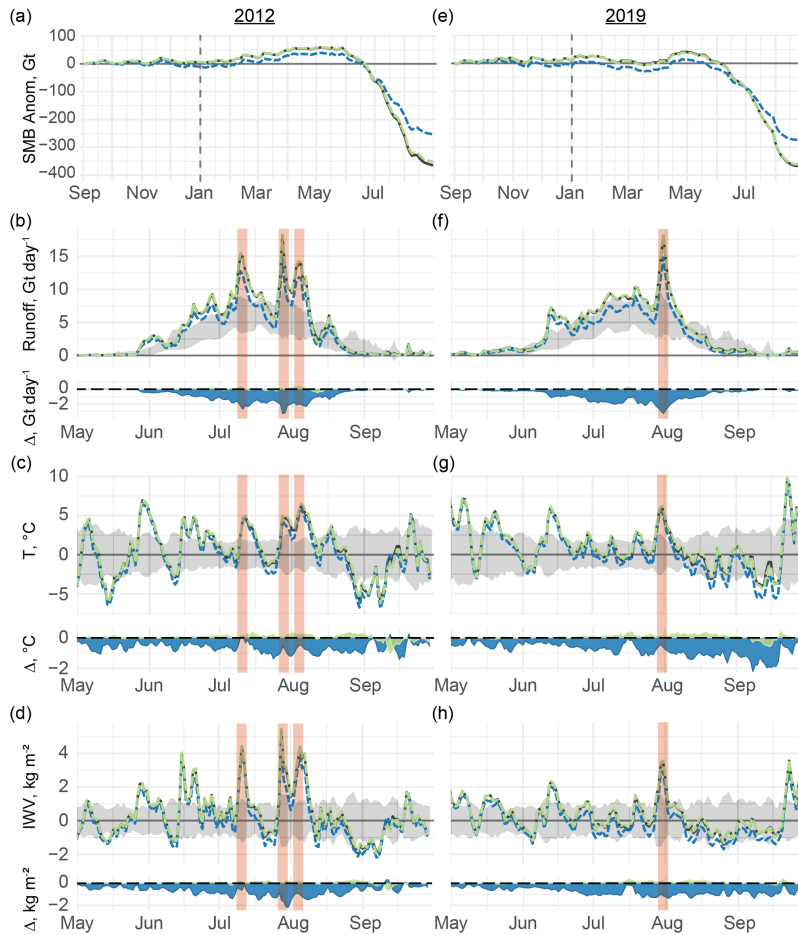
Deleted: Fig. 10

Deleted: PGW1

Deleted: strongly

155 a lesser role during these periods of intense melt. The minimal difference between PGW_{SSC} and the control suggests no
 156 appreciable direct thermodynamic contribution by the observed change in local $SSCs$ to runoff production during these
 157 exceptional melt years.

Deleted: Consistent with the results for the full study period, t
 Deleted: PGW2
 Deleted: sea-surface conditions



158 **Figure 1.** Thermodynamic contribution to surface mass loss during years of exceptional melt. Panels show (a, e) the cumulative SMB
 159 anomaly spanning the Sep–Aug hydrological year alongside (b, f) total daily meltwater runoff, (c, g) mean daily near-surface air temperature

Deleted: 0
 Deleted: GrIS

65 anomaly, and (d, h) mean daily integrated water vapor anomaly during the exceptional melt years of (a–d) 2012 and (e–h) 2019. In all panels,
 66 time series are presented for the control (gray), $PGW_{SSC}^{T,Q}$ (blue dashed), and PGW_{SSC} (green dashed) simulations. Bottom portion of b–d
 67 and f–h shows the difference between each PGW simulation ($PGW_{SSC}^{T,Q}$ blue; PGW_{SSC} green) and the control ($\Delta = PGW - \text{Control}$). Red
 68 vertical shading highlights periods of strong synoptic-scale forcing. Cumulative anomalies in (a, c) calculated with respect to the 1980–1989
 69 reference period. Anomalies in (b–d, f–h) calculated with respect to the entire 2000–2019 study period and represent the spatial average taken
 70 over the entire ice mask for a given variable.
 71

72 Meltwater that exits the ice sheet as runoff is primarily sourced from the ablation zone and is therefore controlled by processes,
 73 such as turbulent heat flux and downward solar radiation (due to the low albedo), that exert a strong influence along the margins
 74 of melt in the high-elevation accumulation zone (with high albedo) is more dependent on longwave radiative effects and
 75 presence of clouds. Given the consistent reduction in water vapor content in $PGW_{SSC}^{T,Q}$ relative to the control (Fig. 11d,h), the
 76 influence of thermodynamic change during these years of extreme mass loss may be more visible in the frequency of melt over
 77 the accumulation zone than for total meltwater runoff.
 78

79 In the control simulation, melt frequencies across the ice sheet were generally greater in 2012 than 2019 (Fig. S6a, c). This is
 80 evident over the southern portion of the ice sheet, where locations above 2500 m in elevation recorded over 40 days of melt in
 81 2012 (Fig. S6a). Melt was also more frequent above ~1500 m over the northern ice sheet in 2012, but 2019 underwent more
 82 frequent melt at lower elevations of the most northern margin of the ice sheet due, in part, to early melt onset and below-
 83 normal snow accumulation which augmented melt through the melt-albedo feedback (Bailey and Hubbard, 2025; Tedesco and
 84 Fettweis, 2020). The difference between $PGW_{SSC}^{T,Q}$ and the control shows that the thermodynamic contribution to melt frequency
 85 was greater in 2019 than in 2012 (Fig. S6b, d). Unlike 2019, intense water vapor transport accompanied the extensive melt
 86 events of 2012 (Hermann et al., 2020; Neff et al., 2014; Tedesco and Fettweis, 2020). Thus, the longwave radiative forcing
 87 necessary for melt over the high-albedo accumulation zone was provided by anomalously high atmospheric moisture supplied
 88 by the large-scale circulation, which likely resulted in less sensitivity to changes in local thermodynamic conditions. In both
 89 years, the greatest differences in melt frequency between $PGW_{SSC}^{T,Q}$ and the control are located just above the ablation zone,
 90 (Fig. S6b, d). The spatial distribution of the differences in melt frequency in $PGW_{SSC}^{T,Q}$ also highlights the thermodynamic
 91 contribution to the maximum elevation of melt extent. This is most evident when considering the decline in melt relative to
 92 the total number of melt days in the control. While the reduction in melt frequency of 1 to 5 days at elevations above ~2000 m
 93 in northern and central Greenland is low compared to other regions of the ice sheet, it is comparable to the total observed
 94 number of melt days simulated by the control (c.f. Fig. S6a, c and b, d), demonstrating that melt over much of the high
 95 accumulation zone would not have occurred if not for recent climate warming. The changes in the number of PGW_{SSC} melt
 96 days relative to the control are minimal and generally do not exhibit a coherent spatial signal (Fig. S6b, d); however, there is
 97 some indication of a decline in 2019 melt frequency over the southwestern ice sheet that is opposed by an increase in melt
 98 frequency above 2000 m (Fig. S6d).

- Deleted: PGW1
- Deleted: PGW2
- Formatted ... [19]
- Formatted ... [20]
- Deleted: PGW1
- Deleted: PGW2
- Formatted ... [21]
- Formatted ... [22]
- Deleted: incoming
- Deleted: of the
- Deleted: ice sheet
- Deleted: GrIS
- Deleted: As was highlighted above, m
- Deleted: PGW1
- Deleted: To investigate this possibility,
- Deleted: 1
- Deleted: quite
- Deleted: 1
- Deleted: GrIS
- Field Code Changed
- Deleted: (Tedesco and Fettweis, 2020)
- Deleted: PGW1
- Deleted: show
- Deleted: 1
- Deleted: PGW1
- Deleted: 1
- Deleted: PGW1
- Deleted: GrIS
- Deleted: melt frequency over high elevations in the context of
- Deleted: simulated by
- Deleted: 1
- Deleted: Contrary to PGW1,
- Deleted: t
- Deleted: PGW2
- Deleted: 1
- Deleted: western slope of the southern
- Deleted: 1

63 **4. Discussion and Conclusions**

64 Much of the work examining the recent increase in Greenland Ice Sheet meltwater runoff has rightfully focused on the role of
65 atmospheric dynamics (Bevis et al., 2019; Fettweis et al., 2013; Hanna et al., 2015, 2016, 2018b, 2022; Hofer et al., 2017).
66 While some have presented evidence of a relationship between global climate change and the shift in summer atmospheric
67 circulation that has promoted melt of the ice sheet (Liu et al., 2016; Preece et al., 2023b; Screen, 2013), a conclusive link
68 remains a subject of investigation. In contrast, the accelerated rate of warming in the Arctic represents a robust climate change
69 signal that has undoubtedly contributed to recent SMB trends (Boers and Rypdal, 2021; Hanna et al., 2008). This work
70 represents, to our knowledge, the first systematic attempt to quantify the contribution of the local change in background
71 thermodynamic conditions to recent surface mass loss.

72
73 Our results indicate that had the large-scale atmospheric circulation that was observed from 2000–2019 occurred under
74 preindustrial thermodynamic background conditions, the magnitude of the cumulative SMB anomaly would have been reduced
75 by over 62% (Fig. 4). The mechanisms by which local thermodynamic background conditions contribute to SMB change
76 appear to be dominated by longwave radiative effects stemming from the water vapor feedback. The amplified rate of warming
77 in the Arctic has augmented surface runoff by promoting an increase in atmospheric moisture and associated downward
78 longwave radiation (Fig. 9a, e and 7b, f), which disproportionately increases daily minimum temperatures (Fig. 9c, g). These
79 results are consistent with Orsi et al. (2017), which identifies a positive trend in 1982–2011 surface air temperature
80 reconstructed from borehole temperature measurements at the North Greenland Eemian Ice Drilling site in northwest
81 Greenland. They point to an increase in downward longwave flux and associated feedbacks as the primary contributor to the
82 warming trend. Likewise, Noël et al. (2019) show that an increase in downward longwave radiation has caused a
83 disproportionate increase in surface runoff from the northern drainages by promoting melt and expanding the ablation zone in
84 this region of high albedo, and by increasing daily minimum temperatures, which reduces meltwater refreeze within the firn
85 layer. While the authors point to the advection of moisture-rich air to the northern ice sheet by anomalously anticyclonic
86 summer circulation over Greenland, the results of this analysis suggest that the increase in background temperature constitutes
87 an important contribution to this mechanism on its own.

88
89 The ~62% reduction, which is conditional on the ERA5 2000–2019 circulation occurring under preindustrial thermodynamic
90 conditions, does not imply that atmospheric circulation is only responsible for 38% of the observed impact on SMB, as the
91 individual contributions of atmospheric dynamics and thermodynamics should sum to the total change in SMB relative to what
92 it would have been if neither an increased frequency of Greenland blocking nor anthropogenic warming had occurred. Given
93 that the ice sheet maintained a positive cumulative SMB anomaly through 2009 under the preindustrial thermodynamic
94 background conditions imposed in $P_{SSC}^{T,Q}$, it is possible that the cumulative anomaly may have remained positive through
95 the end of the study period if not for the increased frequency of anomalous anticyclones. Thus, relative to this hypothetical

- Deleted: ,
- Deleted: pronounced
- Deleted: GrIS
- Deleted: in facilitating this change
- Deleted: GrIS
- Deleted: (Liu et al., 2016; Preece et al., 2023b; Screen, 2013)
- Field Code Changed
- Deleted: GrIS
- Deleted: GrIS
- Deleted: recent atmospheric dynamical forcing
- Deleted: in a preindustrial climate
- Deleted: surface mass loss
- Deleted: from the GrIS
- Deleted:
- Deleted: , highlighting the substantial contribution of external climate forcing
- Deleted: content
- Deleted: welling
- Deleted: Combined with increased SHF along the ice sheet margins of the GrIS (Fig. 7c, g), these changes have reduced the surface albedo (Fig. 9d, h), further increasing meltwater runoff (Fig. 6a, S4).
- Deleted: the recent findings of
- Deleted: , who
- Deleted: elling
- Deleted: of the GrIS
- Deleted:
- Deleted: efficiently
- Deleted: as well as
- Deleted: ¶
- Deleted: in surface mass loss
- Deleted: conditions presented here
- Deleted: GrIS
- Deleted: GrIS
- Deleted: PGW1
- Deleted: high-amplitude circulation patterns

31 preindustrial climate with more typical atmospheric circulation, the total change in SMB would be greater than the magnitude
 32 of the negative anomalies presented in Fig. 4 and the contribution of atmospheric circulation to this total change would exceed
 33 38%. Indeed, using an earth system model to nudge the wind field toward observed conditions while maintaining constant
 34 external forcing, Topál et al. (2022) showed that changes in atmospheric circulation explained 56% of the increase in surface
 35 air temperature over Greenland from 1990 to 2012. Likewise, using historical data and a circulation analogue technique,
 36 Fettweis et al. (2013) found that the shift in summer circulation explained ~70% of the 1993–2012 warming at 700 hPa over
 37 Greenland. Speaking more directly to mass loss, Delhasse et al. (2018) compared output from MAR forced by perturbed
 38 reanalysis data from the recent period of increased Greenland blocking against simulations forced by output from GCMs which
 39 have collectively failed to capture this change in circulation (Delhasse et al., 2021; Hanna et al., 2018a). Their results suggest
 40 that if the recent anomalous circulation persists into the future, the ice sheet will undergo more than twice the surface mass
 41 loss that is currently projected by GCMs. Thus, understanding this circulation change and why it is not represented in climate
 42 models must be a top priority for accurate projections of Greenland Ice Sheet mass loss.

43
 44 The contribution of local thermodynamic background conditions to total surface mass loss during the exceptional melt years
 45 of 2012 and 2019 was less than half that which was observed for the entire 2000–2019 study period (c.f. Fig. 4 and 11a, e),
 46 suggesting that the relative thermodynamic contribution is reduced during periods of strong large-scale atmospheric forcing.
 47 This is also evident over synoptic timescales, where the difference in surface air temperature between $PGW_{SSC}^{T,Q}$ and the control
 48 is minimized on days of exceptional surface runoff; rather, the greatest differences in surface temperature emerge during
 49 periods encompassing temporal minima in air temperature (Fig. 1d). This likely reflects the increased contribution of remotely
 50 sourced heat and moisture during periods of strong large-scale forcing, which would reduce the relative importance of the
 51 longwave radiative effects that typify the response to changes in the thermodynamic background state. In other words, recent
 52 local thermodynamic change around Greenland appears to have promoted surface runoff by raising the floor of the temperature
 53 distribution more so than by exacerbating warm extremes. This signal may be due in part to biases inherent to the PGW
 54 approach. The application of a monthly mean climate perturbation may underrepresent the true change in air temperature and
 55 water vapor concentration during extreme events such as the blocking episodes and attendant atmospheric rivers that have
 56 promoted melt of the ice sheet. While the thermodynamic fields are free to adjust in accordance with any relevant nonlinear
 57 processes within the MAR integration domain, it is likely that any biases at the model boundaries would be conveyed to the
 58 ice sheet to some extent. Despite these shortcomings, the PGW method of downscaling is recognized as an effective means of
 59 isolating the thermodynamic component of climate change (Gutmann et al., 2018; Lackmann, 2015; Mallard et al., 2013;
 60 Rasmussen et al., 2020)—an approach that has been advocated particularly in cases of extreme events for which the governing
 61 dynamics are not well represented in the models (Lloyd and Oreskes, 2018; Trenberth et al., 2015), which is true of both
 62 atmospheric rivers and atmospheric blocking (Delhasse et al., 2021; Hanna et al., 2018a; Wang et al., 2023; Woollings et al.,
 63 2018).

Deleted: ,

Deleted: GrIS

Deleted: GrIS

Deleted: demonstrating

Deleted: by the local thermodynamic state

Deleted: PGW1

Deleted: ly high-volume

Deleted: appear to

Deleted: 0

Deleted: pattern of influence

Deleted: —

Deleted: ing

Deleted: of the background thermodynamic state—as well as the efficacy ...

Deleted: in regulating minimum temperatures

Deleted: GrIS

81 The same large-scale atmospheric conditions that typify our control period and have encouraged mass loss have also fostered
82 below-normal sea ice in the region (Ballinger et al., 2018; Ogi and Wallace, 2007; Stroeve et al., 2017). Thus, the 1880–1899
83 sea ice climatology that we prescribe here may often exceed the SIC that would have occurred if the recently observed
84 atmospheric circulation had occurred under preindustrial conditions. Recognizing this potential bias, our results likely
85 represent an aggressive estimate of the contribution of SSCs to recent surface mass loss. Even so, this analysis reveals minimal
86 direct thermodynamic contribution by local SSCs. Not only does this support previous work showing low SMB sensitivity to
87 adjacent SSCs due to the barrier to onshore advection from the marine layer presented by consistent katabatic outflow over the
88 ice sheet (Hanna et al., 2009, 2014; Noël et al., 2014), but it also shows that any bias due to our treatment of SSCs likely had
89 a negligible impact on our estimate of the total local thermodynamic contribution.

91 Regarding the hypothesis of Stroeve et al. (2017) that declining SIC may promote earlier melt onset thereby preconditioning
92 the ice sheet for greater meltwater production later in the season, our results suggests limited direct thermodynamic impact of
93 local SSCs on recent surface melt and no discernable impact on melt timing (Fig. 4 and 10). There are several plausible
94 reasons for this apparent disparity. First, our interpretation assumes that SSCs and ocean-atmosphere coupling are accurately
95 represented by the model. Gridded climate datasets, with their relatively coarse spatial resolution, are less accurate in areas
96 that rely more heavily on spatial interpolation, such as along coastlines and near the sea ice front where in-situ observations
97 are less frequent (Hanna et al., 2006; Hurrell et al., 2008; Yang et al., 2021). This could degrade model representation of ocean-
98 atmosphere coupling; however, the disparities among various gridded SST and SIC datasets are generally much smaller than
99 the long-term trends (Yang et al., 2021) and, therefore, should exert minimal influence on the signal that we seek to quantify.
00 Second, our experimental design did not examine the isolated contribution of changes in the atmospheric fields alone, and it
01 is possible that nonlinear interactions between changes in SSCs and atmospheric thermodynamic fields caused the combined
02 influence in $PW_{SSC}^{T,Q}$ to be greater than the sum of their individual contributions. Lastly, our analysis did not examine any
03 indirect effects via alteration of the large-scale circulation by changes in SSCs. Both model- and observation-based studies
04 have yielded evidence of a link between declining sea ice in Baffin Bay and the observed increase in summer Greenland
05 blocking (Liu et al., 2016; Screen, 2013; Sellevold et al., 2022; Wu et al., 2013). Indeed, Stroeve et al. (2017) found that the
06 statistical relationship between ice sheet melt and Baffin Bay SIC weakened considerably and, consistent with the PW_{SSC}
07 response in Fig. 5c, became more confined to the periphery of the western ice sheet after correcting for the influence of the
08 Greenland blocking. Considered in conjunction with our results, this suggests that this indirect pathway of influence could
09 help explain the statistical relationship between SSCs and early melt onset.

11 Because MAR assumes a fixed ice sheet geometry, the results presented herein strictly describe the thermodynamic influence
12 on the SMB of the ice sheet; however, surface runoff and solid ice dynamics are not independent. Strong pulses of meltwater
13 can cause rapid drainage through moulins that overwhelms the subglacial drainage network (Chu, 2014; Schoof, 2010), causing
14 a surge in ice velocity that increases glacial discharge and accelerates ice sheet thinning (Andersen et al., 2011; Chu, 2014;

Deleted: It is important to note that t

Deleted: GrIS

Deleted:

Deleted: (Ballinger et al., 2018; Ogi and Wallace, 2007; Stroeve et al., 2017)

Field Code Changed

Deleted: sea-surface conditions

Deleted: GrIS

Deleted: a

Deleted: influence

Deleted: sea-sea surface conditions

Deleted: sea-surface conditions

Deleted: to recent surface mass loss

Deleted: It should also be noted that w

Deleted: While this study quantified the direct contribution of changes in local thermodynamic and sea-surface conditions to surface mass loss, it has been posited that these changes may also contribute to GrIS mass loss indirectly by promoting the observed shift to more persistent atmospheric circulation patterns over Greenland. For example, several theoretical frameworks predict that persistent circulation states may become more common during summer under Arctic amplification (Coumou et al., 2014, 2018; Francis and Vavrus, 2012), and previous work has linked persistent ridging over Greenland to reductions in sea ice and North American snow cover extent (Preece et al., 2023b).

Deleted: Contrary to the hypothesis put forth by Stroeve et al. (2017) that higher SST and lower SIC may promote earlier melt onset in the spring which acts to precondition the ice sheet for later melt, the evidence here suggests very limited impact of sea-surface conditions on recent GrIS surface melt volume and no discernable impact on seasonal melt timing (Fig. 4 and 10). In fact, the little impact by sea-surface conditions that does occur is maximized later in the melt season when ocean-atmosphere heat exchange is greater than during spring (Fig. 6, 7, 9) (Screen, 2017). However, when considering the change in atmospheric thermodynamic fields (i.e., $PW_{SSC}^{T,Q}$), these results show an advance in melt onset and an even greater delay in freeze onset in response to a warming atmosphere that has led to an overall lengthening of the melt season (Fig. 10).

Deleted: GrIS

Deleted: . The consequent buildup of pressure increases basal sliding, ...

.56 Schoof, 2010). Thus, it is likely that the thermodynamic influence on surface melt documented here has indirectly contributed
.57 further to sea-level rise via its impact on ice sheet dynamics. Regardless, these results demonstrate that while the shift in
.58 summer atmospheric circulation over Greenland has been key to the acceleration of runoff from the ice sheet, the change in
.59 the background thermodynamic state under Arctic amplification has markedly enhanced the observed surface mass loss beyond
.60 that which would have occurred if not for anthropogenic climate change.

Deleted: GrIS

Deleted: GrIS

.61 **Code and Data Availability**

.62 MAR data from this study are available through the Arctic Data Center (Preece et al., 2023a). ERA5 reanalysis data used to
.63 force the model can be accessed through the Copernicus Climate Data Store (Copernicus Climate Change Service, 2018).
.64 CESM-LE data used adjust the boundary conditions are available through the National Science Foundation (NSF) National
.65 Center for Atmospheric Research (NCAR) Research Data Archive (Kay et al., 2021). Merged Hadley-OI SIC and SST fields
.66 are hosted through Zenodo (Hurrell, James W. et al., 2020).

.67 **Author Contribution**

.68 JP, TM, and PA conceptualized the study. JP, PA, and GK designed the model experiments. JP, PA, and XF performed the
.69 model simulations. TM and MT led the project administration and funding acquisition. MT and PA supplied the computing
.70 resources. JP performed the formal analysis and prepared the manuscript in consultation with all co-authors.

.71 **Competing Interests**

.72 At least one of the (co-)authors is a member of the editorial board of The Cryosphere.

.73 **Acknowledgements**

.74 Computing resources to perform the MAR simulations were provided by the Lamont-Doherty Earth Observatory.

.75 **Financial Support**

.76 This work was supported by NSF Arctic Systems Science award number 1900324, Strategic Environmental Research and
.77 Development Program project number RC18-1658, NASA award 80NSSC17K0351 and Heising Simons Foundation award #
.78 HSFOUNF 2019 - 1160. G.J.K. acknowledges support from the U.S. Department of Energy (DOE) Regional and Global Model
.79 Analysis (RGMA) Program (DE-SC0021209).

82 **References**

- 83 [Amory, C., Kittel, C., Le Toumelin, L., Agosta, C., Delhasse, A., Favier, V., and Fettweis, X.: Performance of MAR \(v3.11\)](#)
84 [in simulating the drifting-snow climate and surface mass balance of Adélie Land, East Antarctica, *Geoscientific Model*](#)
85 [Development](#), 14, 3487–3510, <https://doi.org/10.5194/gmd-14-3487-2021>, 2021.
- 86 [Andersen, M. L., Nettles, M., Elosegui, P., Larsen, T. B., Hamilton, G. S., and Stearns, L. A.: Quantitative estimates of velocity](#)
87 [sensitivity to surface melt variations at a large Greenland outlet glacier, *Journal of Glaciology*](#), 57, 609–620,
88 <https://doi.org/10.3189/002214311797409785>, 2011.
- 89 [Bailey, H. and Hubbard, A.: Snow Mass Recharge of the Greenland Ice Sheet Fueled by Intense Atmospheric River,](#)
90 [Geophysical Research Letters](#), 52, e2024GL110121, <https://doi.org/10.1029/2024GL110121>, 2025.
- 91 [Ballinger, T. J., Hanna, E., Hall, R. J., Miller, J., Ribergaard, M. H., and Høyer, J. L.: Greenland coastal air temperatures linked](#)
92 [to Baffin Bay and Greenland Sea ice conditions during autumn through regional blocking patterns, *Clim Dyn*](#), 50, 83–100,
93 <https://doi.org/10.1007/s00382-017-3583-3>, 2018.
- 94 [Ballinger, T. J., Mote, T. L., Mattingly, K., Bliss, A. C., Hanna, E., van As, D., Prieto, M., Gharehchahi, S., Fettweis, X., Noël,](#)
95 [B., Smeets, P. C. J. P., Ribergaard, M. H., and Cappelen, J.: Greenland Ice Sheet late-season melt: Investigating multi-scale](#)
96 [drivers of K-transect events, *The Cryosphere Discuss.*](#), 1–23, <https://doi.org/10.5194/tc-2018-285>, 2019.
- 97 [Bennartz, R., Shupe, M. D., Turner, D. D., Walden, V. P., Steffen, K., Cox, C. J., Kulie, M. S., Miller, N. B., and Pettersen,](#)
98 [C.: July 2012 Greenland melt extent enhanced by low-level liquid clouds, *Nature*](#), 496, 83–86,
99 <https://doi.org/10.1038/nature12002>, 2013.
- 00 [Bevis, M., Harig, C., Khan, S. A., Brown, A., Simons, F. J., Willis, M., Fettweis, X., Broeke, M. R., van den, Madsen, F. B.,](#)
01 [Kendrick, E., Caccamise, D. J., Dam, T., van, Knudsen, P., and Nylen, T.: Accelerating changes in ice mass within Greenland,](#)
02 [and the ice sheet’s sensitivity to atmospheric forcing, *PNAS*](#), 116, 1934–1939, <https://doi.org/10.1073/pnas.1806562116>, 2019.
- 03 [Boers, N. and Rypdal, M.: Critical slowing down suggests that the western Greenland Ice Sheet is close to a tipping point,](#)
04 [Proceedings of the National Academy of Sciences](#), 118, e2024192118, <https://doi.org/10.1073/pnas.2024192118>, 2021.
- 05 [Box, J. E., Cressie, N., Bromwich, D. H., Jung, J.-H., Van Den Broeke, M., Van Angelen, J. H., Forster, R. R., Miège, C.,](#)
06 [Mosley-Thompson, E., Vinther, B., and McConnell, J. R.: Greenland Ice Sheet Mass Balance Reconstruction. Part I: Net Snow](#)
07 [Accumulation \(1600–2009\), *Journal of Climate*](#), 26, 3919–3934, <https://doi.org/10.1175/JCLI-D-12-00373.1>, 2013.
- 08 [Box, J. E., Wehrlé, A., van As, D., Fausto, R. S., Kjeldsen, K. K., Dachauer, A., Ahlstrøm, A. P., and Picard, G.: Greenland](#)
09 [Ice Sheet Rainfall, Heat and Albedo Feedback Impacts From the Mid-August 2021 Atmospheric River, *Geophysical Research*](#)
10 [Letters](#), 49, e2021GL097356, <https://doi.org/10.1029/2021GL097356>, 2022.
- 11 [Box, J. E., Nielsen, K. P., Yang, X., Niwano, M., Wehrlé, A., van As, D., Fettweis, X., Koltzow, M. A. Ø., Palmason, B.,](#)
12 [Fausto, R. S., van den Broeke, M. R., Huai, B., Ahlstrøm, A. P., Langley, K., Dachauer, A., and Noël, B.: Greenland ice sheet](#)
13 [rainfall climatology, extremes and atmospheric river rapids, *Meteorological Applications*](#), 30, e2134,
14 <https://doi.org/10.1002/met.2134>, 2023.
- 15 [van den Broeke, M. R., Bamber, J., Ettema, J., Rignot, E., Schrama, E., Berg, W. J. van de, Meijgaard, E. van, Velicogna, I.,](#)
16 [and Wouters, B.: Partitioning Recent Greenland Mass Loss, *Science*](#), 326, 984–986, <https://doi.org/10.1126/science.1178176>,
- 17 [2009a.](#)

Formatted: Bibliography, Adjust space between Latin and Asian text, Adjust space between Asian text and numbers

18 [van den Broeke, M. R., Smeets, P., and Ettema, J.: Surface layer climate and turbulent exchange in the ablation zone of the](#)
19 [west Greenland ice sheet, International Journal of Climatology, 29, 2309–2323, <https://doi.org/10.1002/joc.1815>, 2009b.](#)

20 [van den Broeke, M. R., Enderlin, E. M., Howat, I. M., Kuipers Munneke, P., Noël, B. P. Y., van de Berg, W. J., van Meijgaard,](#)
21 [E., and Wouters, B.: On the recent contribution of the Greenland ice sheet to sea level change, The Cryosphere, 10, 1933–](#)
22 [1946, <https://doi.org/10.5194/tc-10-1933-2016>, 2016.](#)

23 [Bromwich, D. H., Cullather, R. I., Chen, Q., and Csathó, B. M.: Evaluation of recent precipitation studies for Greenland Ice](#)
24 [Sheet, Journal of Geophysical Research: Atmospheres, 103, 26007–26024, <https://doi.org/10.1029/98JD02278>, 1998.](#)

25 [Brun, E., Martin, E., Simon, V., Gendre, C., and Coléou, C.: An Energy and Mass Model of Snow Cover Suitable for](#)
26 [Operational Avalanche Forecasting, J. Glaciol., 35, 333, <https://doi.org/10.1017/S0022143000009254>, 1989.](#)

27 [Brun, E., David, P., Sudul, M., and Brunot, G.: A numerical model to simulate snow-cover stratigraphy for operational](#)
28 [avalanche forecasting, Journal of Glaciology, 38, 13–22, <https://doi.org/10.3189/S0022143000009552>, 1992.](#)

29 [Caesar, L., Rahmstorf, S., Robinson, A., Feulner, G., and Saba, V.: Observed fingerprint of a weakening Atlantic Ocean](#)
30 [overturning circulation, Nature, 556, 191–196, <https://doi.org/10.1038/s41586-018-0006-5>, 2018.](#)

31 [Cattiaux, J., Peings, Y., Saint-Martin, D., Trou-Kechout, N., and Vavrus, S. J.: Sinuosity of midlatitude atmospheric flow in a](#)
32 [warming world, Geophysical Research Letters, 43, 8259–8268, <https://doi.org/10.1002/2016GL070309>, 2016.](#)

33 [Cazenave, A., Palanisamy, H., and Ablain, M.: Contemporary sea level changes from satellite altimetry: What have we](#)
34 [learned? What are the new challenges?, Advances in Space Research, 62, 1639–1653,](#)
35 [https://doi.org/10.1016/j.asr.2018.07.017, 2018.](#)

36 [Chu, V. W.: Greenland ice sheet hydrology: A review, Progress in Physical Geography: Earth and Environment, 38, 19–54,](#)
37 [https://doi.org/10.1177/0309133313507075, 2014.](#)

38 [Chung, E., Ha, K., Timmermann, A., Stuecker, M. F., Bodai, T., and Lee, S.: Cold-Season Arctic Amplification Driven by](#)
39 [Arctic Ocean-Mediated Seasonal Energy Transfer, Earth's Future, 9, <https://doi.org/10.1029/2020ef001898>, 2021.](#)

40 [Clausen, H. B., Gundestrup, N. S., Johnsen, S. J., Bindschadler, R., and Zwally, J.: Glaciological Investigations in the Crête](#)
41 [Area, Central Greenland: A Search for a new Deep-Drilling Site, Annals of Glaciology, 10, 10–15,](#)
42 [https://doi.org/10.3189/S0260305500004080, 1988.](#)

43 [Cohen, J., Screen, J. A., Furtado, J. C., Barlow, M., Whittleston, D., Coumou, D., Francis, J., Dethloff, K., Entekhabi, D.,](#)
44 [Overland, J., and Jones, J.: Recent Arctic amplification and extreme mid-latitude weather, Nature Geoscience, 7, 627–637,](#)
45 [https://doi.org/10.1038/ngeo2234, 2014.](#)

46 [Copernicus Climate Change Service: ERA5 hourly data on pressure levels from 1940 to present,](#)
47 [https://doi.org/10.24381/CDS.BD0915C6, 2018.](#)

48 [Coumou, D., Lehmann, J., and Beckmann, J.: The weakening summer circulation in the Northern Hemisphere mid-latitudes,](#)
49 [Science, 348, 324–327, <https://doi.org/10.1126/science.1261768>, 2015.](#)

50 [Coumou, D., Di Capua, G., Vavrus, S., Wang, L., and Wang, S.: The influence of Arctic amplification on mid-latitude summer](#)
51 [circulation, Nat Commun, 9, 2959, <https://doi.org/10.1038/s41467-018-05256-8>, 2018.](#)

52 [Cullather, R. I., Andrews, L. C., Croteau, M. J., Digirolamo, N. E., Hall, D. K., Lim, Y.-K., Loomis, B. D., Shuman, C. A.,](#)
53 [and Nowicki, S. M. J.: Anomalous Circulation in July 2019 Resulting in Mass Loss on the Greenland Ice Sheet, *Geophysical*](#)
54 [Research Letters, 47, e2020GL087263, <https://doi.org/10.1029/2020GL087263>, 2020.](#)

55 [Davini, P. and D'Andrea, F.: From CMIP3 to CMIP6: Northern Hemisphere Atmospheric Blocking Simulation in Present and](#)
56 [Future Climate, *Journal of Climate*, 33, 10021–10038, <https://doi.org/10.1175/JCLI-D-19-0862.1>, 2020.](#)

57 [Delhasse, A., Fettweis, X., Kittel, C., Amory, C., and Agosta, C.: Brief communication: Impact of the recent atmospheric](#)
58 [circulation change in summer on the future surface mass balance of the Greenland Ice Sheet, *The Cryosphere*, 12, 3409–3418,](#)
59 [https://doi.org/10.5194/tc-12-3409-2018, 2018.](#)

60 [Delhasse, A., Hanna, E., Kittel, C., and Fettweis, X.: Brief communication: CMIP6 does not suggest any atmospheric blocking](#)
61 [increase in summer over Greenland by 2100, *International Journal of Climatology*, 41, 2589–2596,](#)
62 [https://doi.org/10.1002/joc.6977, 2021.](#)

63 [Di Capua, G. and Coumou, D.: Changes in meandering of the Northern Hemisphere circulation, *Environ. Res. Lett.*, 11,](#)
64 [094028, <https://doi.org/10.1088/1748-9326/11/9/094028>, 2016.](#)

65 [Fausto, R. S., van As, D., Box, J. E., Colgan, W., and Langen, P. L.: Quantifying the Surface Energy Fluxes in South Greenland](#)
66 [during the 2012 High Melt Episodes Using In-situ Observations, *Front. Earth Sci.*, 4, <https://doi.org/10.3389/feart.2016.00082>,](#)
67 [2016a.](#)

68 [Fausto, R. S., van As, D., Box, J. E., Colgan, W., Langen, P. L., and Mottram, R. H.: The implication of nonradiative energy](#)
69 [fluxes dominating Greenland ice sheet exceptional ablation area surface melt in 2012, *Geophysical Research Letters*, 43, 2649–](#)
70 [2658, <https://doi.org/10.1002/2016GL067720>, 2016b.](#)

71 [Fettweis, X., Gallée, H., Lefebvre, F., and van Ypersele, J.-P.: Greenland surface mass balance simulated by a regional climate](#)
72 [model and comparison with satellite-derived data in 1990–1991, *Climate Dynamics*, 24, 623–640,](#)
73 [https://doi.org/10.1007/s00382-005-0010-y, 2005.](#)

74 [Fettweis, X., Hanna, E., Lang, C., Belleflamme, A., Ericum, M., and Gallée, H.: Brief communication: “Important role of the](#)
75 [mid-tropospheric atmospheric circulation in the recent surface melt increase over the Greenland ice sheet.” *The Cryosphere*,](#)
76 [7, 241–248, <https://doi.org/10.5194/tc-7-241-2013>, 2013.](#)

77 [Fettweis, X., Box, J. E., Agosta, C., Amory, C., Kittel, C., Lang, C., van As, D., Machguth, H., and Gallée, H.: Reconstructions](#)
78 [of the 1900–2015 Greenland ice sheet surface mass balance using the regional climate MAR model, *The Cryosphere*, 11,](#)
79 [1015–1033, <https://doi.org/10.5194/tc-11-1015-2017>, 2017.](#)

80 [Fettweis, X., Hofer, S., Krebs-Kanzow, U., Amory, C., Aoki, T., Berends, C. J., Born, A., Box, J. E., Delhasse, A., Fujita, K.,](#)
81 [Gierz, P., Goelzer, H., Hanna, E., Hashimoto, A., Huybrechts, P., Kapsch, M.-L., King, M. D., Kittel, C., Lang, C., Langen,](#)
82 [P. L., Lenaerts, J. T. M., Liston, G. E., Lohmann, G., Mernild, S. H., Mikolajewicz, U., Modali, K., Mottram, R. H., Niwano,](#)
83 [M., Noël, B., Ryan, J. C., Smith, A., Streffing, J., Tedesco, M., van de Berg, W. J., van den Broeke, M., van de Wal, R. S. W.,](#)
84 [van Kampenhout, L., Wilton, D., Wouters, B., Ziemens, F., and Zolles, T.: GrSMBMIP: intercomparison of the modelled 1980–](#)
85 [2012 surface mass balance over the Greenland Ice Sheet, *The Cryosphere*, 14, 3935–3958, <https://doi.org/10.5194/tc-14-3935->](#)
86 [2020, 2020.](#)

87 [Francis, J. A. and Vavrus, S. J.: Evidence linking Arctic amplification to extreme weather in mid-latitudes: ARCTIC LINKS](#)
88 [TO MID-LATITUDE WEATHER, *Geophys. Res. Lett.*, 39, L06801, <https://doi.org/10.1029/2012GL051000>, 2012.](#)

89 [Gallagher, M. R., Shupe, M. D., and Miller, N. B.: Impact of Atmospheric Circulation on Temperature, Clouds, and Radiation](#)
90 [at Summit Station, Greenland, with Self-Organizing Maps, *J. Climate*, 31, 8895–8915, \[https://doi.org/10.1175/JCLI-D-17-\]\(https://doi.org/10.1175/JCLI-D-17-0893.1\)](#)
91 [0893.1, 2018.](#)

92 [Gorter, W., van Angelen, J. H., Lenaerts, J. T. M., and van den Broeke, M. R.: Present and future near-surface wind climate](#)
93 [of Greenland from high resolution regional climate modelling, *Clim Dyn*, 42, 1595–1611, \[https://doi.org/10.1007/s00382-013-\]\(https://doi.org/10.1007/s00382-013-1861-2\)](#)
94 [1861-2, 2014.](#)

95 [Gutmann, E. D., Rasmussen, R. M., Liu, C., Ikeda, K., Bruyere, C. L., Done, J. M., Garré, L., Friis-Hansen, P., and Veldore,](#)
96 [V.: Changes in Hurricanes from a 13-Yr Convection-Permitting Pseudo-Global Warming Simulation, *Journal of Climate*, 31,](#)
97 [3643–3657, <https://doi.org/10.1175/JCLI-D-17-0391.1>, 2018.](#)

98 [Hanna, E., Jónsson, T., Ólafsson, J., and Valdimarsson, H.: Icelandic Coastal Sea Surface Temperature Records Constructed:](#)
99 [Putting the Pulse on Air–Sea–Climate Interactions in the Northern North Atlantic. Part I: Comparison with HadSST1 Open-](#)
00 [Ocean Surface Temperatures and Preliminary Analysis of Long-Term Patterns and Anomalies of SSTs around Iceland, *Journal*](#)
01 [of Climate, 19, 5652–5666, <https://doi.org/10.1175/JCLI3933.1>, 2006.](#)

02 [Hanna, E., Huybrechts, P., Steffen, K., Cappelen, J., Huff, R., Shuman, C., Irvine-Fynn, T., Wise, S., and Griffiths, M.:](#)
03 [Increased Runoff from Melt from the Greenland Ice Sheet: A Response to Global Warming, *J. Climate*, 21, 331–341,](#)
04 [https://doi.org/10.1175/2007JCLI1964.1, 2008.](#)

05 [Hanna, E., Cappelen, J., Fettweis, X., Huybrechts, P., Luckman, A., and Ribergaard, M. H.: Hydrologic response of the](#)
06 [Greenland ice sheet: the role of oceanographic warming, *Hydrological Processes*, 23, 7–30, \[https://doi.org/10.1002/hyp.7090,\]\(https://doi.org/10.1002/hyp.7090\)](#)
07 [2009.](#)

08 [Hanna, E., Jones, J. M., Cappelen, J., Mernild, S. H., Wood, L., Steffen, K., and Huybrechts, P.: The influence of North Atlantic](#)
09 [atmospheric and oceanic forcing effects on 1900–2010 Greenland summer climate and ice melt/runoff, *Int. J. Climatol.*, 33,](#)
10 [862–880, <https://doi.org/10.1002/joc.3475>, 2013.](#)

11 [Hanna, E., Fettweis, X., Mernild, S. H., Cappelen, J., Ribergaard, M. H., Shuman, C. A., Steffen, K., Wood, L., and Mote, T.](#)
12 [L.: Atmospheric and oceanic climate forcing of the exceptional Greenland ice sheet surface melt in summer 2012, *International*](#)
13 [Journal of Climatology, 34, 1022–1037, <https://doi.org/10.1002/joc.3743>, 2014.](#)

14 [Hanna, E., Cropper, T. E., Jones, P. D., Scaife, A. A., and Allan, R.: Recent seasonal asymmetric changes in the NAO \(a](#)
15 [marked summer decline and increased winter variability\) and associated changes in the AO and Greenland Blocking Index,](#)
16 [International Journal of Climatology, 35, 2540–2554, <https://doi.org/10.1002/joc.4157>, 2015.](#)

17 [Hanna, E., Cropper, T. E., Hall, R. J., and Cappelen, J.: Greenland Blocking Index 1851–2015: a regional climate change](#)
18 [signal: Greenland Blocking Index 1851–2015, *Int. J. Climatol.*, 36, 4847–4861, <https://doi.org/10.1002/joc.4673>, 2016.](#)

19 [Hanna, E., Fettweis, X., and Hall, R. J.: Brief communication: Recent changes in summer Greenland blocking captured by](#)
20 [none of the CMIP5 models, *The Cryosphere*, 12, 3287–3292, <https://doi.org/10.5194/tc-12-3287-2018>, 2018a.](#)

21 [Hanna, E., Hall, R. J., Cropper, T. E., Ballinger, T. J., Wake, L., Mote, T., and Cappelen, J.: Greenland blocking index daily](#)
22 [series 1851–2015: Analysis of changes in extremes and links with North Atlantic and UK climate variability and change,](#)
23 [International Journal of Climatology, 38, 3546–3564, <https://doi.org/10.1002/joc.5516>, 2018b.](#)

24 [Hanna, E., Cappelen, J., Fettweis, X., Mernild, S. H., Mote, T. L., Mottram, R., Steffen, K., Ballinger, T. J., and Hall, R. J.:](#)
25 [Greenland surface air temperature changes from 1981 to 2019 and implications for ice-sheet melt and mass-balance change,](#)
26 [International Journal of Climatology, 41, E1336–E1352, <https://doi.org/10.1002/joc.6771>, 2021.](#)

.27 [Hanna, E., Cropper, T. E., Hall, R. J., Cornes, R. C., and Barriendos, M.: Extended North Atlantic Oscillation and Greenland](#)
.28 [Blocking Indices 1800–2020 from New Meteorological Reanalysis, *Atmosphere*, 13, 436,](#)
.29 <https://doi.org/10.3390/atmos13030436>, 2022.

.30 [Hanna, E., Topál, D., Box, J. E., Buzzard, S., Christie, F. D. W., Hvidberg, C., Morlighem, M., De Santis, L., Silvano, A.,](#)
.31 [Colleoni, F., Sasgen, I., Banwell, A. F., van den Broeke, M. R., DeConto, R., De Rydt, J., Goelzer, H., Gossart, A.,](#)
.32 [Gudmundsson, G. H., Lindbäck, K., Miles, B., Mottram, R., Pattyn, F., Reese, R., Rignot, E., Srivastava, A., Sun, S., Toller,](#)
.33 [J., Tuckett, P. A., and Ultee, L.: Short- and long-term variability of the Antarctic and Greenland ice sheets, *Nat Rev Earth*](#)
.34 [Environ, 5, 193–210, <https://doi.org/10.1038/s43017-023-00509-7>, 2024.](#)

.35 [Henderson, G. R., Barrett, B. S., Wachowicz, L. J., Mattingly, K. S., Preece, J. R., and Mote, T. L.: Local and Remote](#)
.36 [Atmospheric Circulation Drivers of Arctic Change: A Review, *Frontiers in Earth Science*, 9,](#)
.37 <https://doi.org/10.3389/feart.2021.709896>, 2021.

.38 [Hermann, M., Papritz, L., and Wernli, H.: A Lagrangian analysis of the dynamical and thermodynamic drivers of large-scale](#)
.39 [Greenland melt events during 1979–2017, *Weather and Climate Dynamics*, 1, 497–518, \[2020\]\(https://doi.org/10.5194/wcd-1-497-
.40 <a href=\), 2020.](#)

.41 [Hofer, S., Tedstone, A. J., Fettweis, X., and Bamber, J. L.: Decreasing cloud cover drives the recent mass loss on the Greenland](#)
.42 [Ice Sheet, *Science Advances*, 3, e1700584, <https://doi.org/10.1126/sciadv.1700584>, 2017.](#)

.43 [Horwath, M., Gutknecht, B. D., Cazenave, A., Palanisamy, H. K., Marti, F., Marzeion, B., Paul, F., Le Bris, R., Hogg, A. E.,](#)
.44 [Otosaka, I., Shepherd, A., Döll, P., Cáceres, D., Müller Schmied, H., Johannessen, J. A., Nilsen, J. E. Ø., Raj, R. P., Forsberg,](#)
.45 [R., Sandberg Sørensen, L., Barletta, V. R., Simonsen, S. B., Knudsen, P., Andersen, O. B., Rannald, H., Rose, S. K., Merchant,](#)
.46 [C. J., Macintosh, C. R., von Schuckmann, K., Novotny, K., Groh, A., Restano, M., and Benveniste, J.: Global sea-level budget](#)
.47 [and ocean-mass budget, with a focus on advanced data products and uncertainty characterisation, *Earth System Science Data*,](#)
.48 [14, 411–447, <https://doi.org/10.5194/essd-14-411-2022>, 2022.](#)

.49 [Hurrell, J. W., Hack, J. J., Shea, D., Caron, J. M., and Rosinski, J.: A New Sea Surface Temperature and Sea Ice Boundary](#)
.50 [Dataset for the Community Atmosphere Model, *Journal of Climate*, 21, 5145–5153, <https://doi.org/10.1175/2008JCLI2292.1>,](#)
.51 [2008.](#)

.52 [Hurrell, James W., Phillips, Adam, and Shea, Dennis: Merged Hadley-OI sea surface temperature and sea ice concentration](#)
.53 [data set, <https://doi.org/10.5065/R33V-SV91>, 2020.](#)

.54 [Kawase, H., Yoshikane, T., Hara, M., Ailikun, B., Kimura, F., and Yasunari, T.: Downscaling of the Climatic Change in the](#)
.55 [Mei-yu Rainband in East Asia by a Pseudo Climate Simulation Method, *SOLA*, 4, 73–76, \[019\]\(https://doi.org/10.2151/sola.2008-
.56 <a href=\), 2008.](#)

.57 [Kay, J., Deser, C., Phillips, A., and Simpson, I.: CESM1 Large Ensemble Community Project,](#)
.58 <https://doi.org/10.5065/D6J101D1>, 2021.

.59 [Kay, J. E., Deser, C., Phillips, A., Mai, A., Hannay, C., Strand, G., Arblaster, J. M., Bates, S. C., Danabasoglu, G., Edwards,](#)
.60 [J., Holland, M., Kushner, P., Lamarque, J.-F., Lawrence, D., Lindsay, K., Middleton, A., Munoz, E., Neale, R., Oleson, K.,](#)
.61 [Polvani, L., and Vertenstein, M.: The Community Earth System Model \(CESM\) Large Ensemble Project: A Community](#)
.62 [Resource for Studying Climate Change in the Presence of Internal Climate Variability, *Bulletin of the American*](#)
.63 [Meteorological Society, 96, 1333–1349, <https://doi.org/10.1175/BAMS-D-13-00255.1>, 2015.](#)

.64 [Khan, S. A., Aschwanden, A., Bjørk, A. A., Wahr, J., Kjeldsen, K. K., and Kjær, K. H.: Greenland ice sheet mass balance: a](#)
.65 [review, *Rep. Prog. Phys.*, 78, 046801, <https://doi.org/10.1088/0034-4885/78/4/046801>, 2015.](#)

66 [Kimura, F. and Kitoh, A.: Downscaling by pseudo global warming method, The Final Report of ICCAP, 4346, 2007.](#)

67 [Kjeldsen, K. K., Korsgaard, N. J., Bjørk, A. A., Khan, S. A., Box, J. E., Funder, S., Larsen, N. K., Bamber, J. L., Colgan, W.,](#)
68 [van den Broeke, M., Siggaard-Andersen, M.-L., Nuth, C., Schomacker, A., Andresen, C. S., Willerslev, E., and Kjær, K. H.:](#)
69 [Spatial and temporal distribution of mass loss from the Greenland Ice Sheet since AD 1900, Nature, 528, 396–400,](#)
70 <https://doi.org/10.1038/nature16183>, 2015.

71 [Kornhuber, K. and Tamarin-Brodsky, T.: Future Changes in Northern Hemisphere Summer Weather Persistence Linked to](#)
72 [Projected Arctic Warming, Geophysical Research Letters, 48, e2020GL091603, https://doi.org/10.1029/2020GL091603,](#)
73 [2021.](#)

74 [Lackmann, G. M.: Hurricane Sandy before 1900 and after 2100, Bull. Amer. Meteor. Soc., 96, 547–560,](#)
75 <https://doi.org/10.1175/BAMS-D-14-00123.1>, 2015.

76 [Lefebvre, F., Fettweis, X., Gallée, H., Van Ypersele, J.-P., Marbaix, P., Greuell, W., and Calanca, P.: Evaluation of a high-](#)
77 [resolution regional climate simulation over Greenland, Climate Dynamics, 25, 99–116, https://doi.org/10.1007/s00382-005-](#)
78 [0005-8](#), 2005.

79 [Lenaerts, J. T. M., Medley, B., van den Broeke, M. R., and Wouters, B.: Observing and Modeling Ice Sheet Surface Mass](#)
80 [Balance, Reviews of Geophysics, 57, 376–420, https://doi.org/10.1029/2018RG000622](#), 2019.

81 [Liu, J., Chen, Z., Francis, J., Song, M., Mote, T., and Hu, Y.: Has Arctic Sea Ice Loss Contributed to Increased Surface Melting](#)
82 [of the Greenland Ice Sheet?, J. Climate, 29, 3373–3386, https://doi.org/10.1175/JCLI-D-15-0391.1](#), 2016.

83 [Lloyd, E. A. and Oreskes, N.: Climate Change Attribution: When Is It Appropriate to Accept New Methods?, Earth's Future,](#)
84 [6, 311–325, https://doi.org/10.1002/2017EF000665](#), 2018.

85 [Mallard, M. S., Lackmann, G. M., Aiyyer, A., and Hill, K.: Atlantic Hurricanes and Climate Change. Part I: Experimental](#)
86 [Design and Isolation of Thermodynamic Effects, Journal of Climate, 26, 4876–4893, https://doi.org/10.1175/JCLI-D-12-](#)
87 [00182.1](#), 2013.

88 [Mankoff, K. D., Colgan, W., Solgaard, A., Karlsson, N. B., Ahlstrøm, A. P., As, D. V., Box, J. E., Khan, S. A., Kjeldsen, K.,](#)
89 [Mouginot, J., and Fausto, R. S.: Greenland Ice Sheet solid ice discharge from 1986 through 2017, Earth System Science](#)
90 [Data, 11, 769–786, https://doi.org/10.5194/essd-11-769-2019](#), 2019.

91 [Mattingly, K. S., Ramseyer, C. A., Rosen, J. J., Mote, T. L., and Muthyala, R.: Increasing water vapor transport to the](#)
92 [Greenland Ice Sheet revealed using self-organizing maps, Geophysical Research Letters, 43, 9250–9258,](#)
93 <https://doi.org/10.1002/2016GL070424>, 2016.

94 [Mattingly, K. S., Mote, T. L., and Fettweis, X.: Atmospheric River Impacts on Greenland Ice Sheet Surface Mass Balance,](#)
95 [Journal of Geophysical Research: Atmospheres, 123, 8538–8560, https://doi.org/10.1029/2018JD028714](#), 2018.

96 [Meese, D. A., Gow, A. J., Grootes, P., Mayewski, P. A., Ram, M., Stuiver, M., Taylor, K. C., Waddington, E. D., and Zielinski,](#)
97 [G. A.: The Accumulation Record from the GISP2 Core as an Indicator of Climate Change Throughout the Holocene, Science,](#)
98 [266, 1680–1682](#), 1994.

99 [Mote, T. L.: Mid-tropospheric circulation and surface melt on the Greenland ice sheet. Part I: atmospheric teleconnections,](#)
00 [International Journal of Climatology, 18, 111–129, https://doi.org/10.1002/\(SICI\)1097-0088\(199802\)18:2%253C111::AID-](#)
01 [JOC227%253E3.0.CO;2-X](#), 1998.

02 [Mote, T. L.: Greenland surface melt trends 1973–2007: Evidence of a large increase in 2007, *Geophysical Research Letters*,](https://doi.org/10.1029/2007GL031976)
03 [34, https://doi.org/10.1029/2007GL031976, 2007.](https://doi.org/10.1029/2007GL031976)

04 [Mouginot, J., Rignot, E., Bjørk, A. A., van den Broeke, M. R., Millan, R., Morlighem, M., Noël, B., Scheuchl, B., and Wood,](https://doi.org/10.1073/pnas.1904242116)
05 [M.: Forty-six years of Greenland Ice Sheet mass balance from 1972 to 2018, *PNAS*, 116, 9239–9244,](https://doi.org/10.1073/pnas.1904242116)
06 [https://doi.org/10.1073/pnas.1904242116, 2019.](https://doi.org/10.1073/pnas.1904242116)

07 [Neff, W., Compo, G. P., Martin Ralph, F., and Shupe, M. D.: Continental heat anomalies and the extreme melting of the](https://doi.org/10.1002/2014JD021470)
08 [Greenland ice surface in 2012 and 1889: Melting of Greenland in 1889 and 2012, *J. Geophys. Res. Atmos.*, 119, 6520–6536,](https://doi.org/10.1002/2014JD021470)
09 [https://doi.org/10.1002/2014JD021470, 2014.](https://doi.org/10.1002/2014JD021470)

10 [Nghiem, S. V., Hall, D. K., Mote, T. L., Tedesco, M., Albert, M. R., Keegan, K., Shuman, C. A., DiGirolamo, N. E., and](https://doi.org/10.1029/2012GL053611)
11 [Neumann, G.: The extreme melt across the Greenland ice sheet in 2012, *Geophysical Research Letters*, 39,](https://doi.org/10.1029/2012GL053611)
12 [https://doi.org/10.1029/2012GL053611, 2012.](https://doi.org/10.1029/2012GL053611)

13 [Noël, B., Fettweis, X., van de Berg, W. J., van den Broeke, M. R., and Erpicum, M.: Sensitivity of Greenland Ice Sheet surface](https://doi.org/10.5194/tc-8-1871-2014)
14 [mass balance to perturbations in sea surface temperature and sea ice cover: a study with the regional climate model MAR, *The*](https://doi.org/10.5194/tc-8-1871-2014)
15 [Cryosphere](https://doi.org/10.5194/tc-8-1871-2014), 8, 1871–1883, <https://doi.org/10.5194/tc-8-1871-2014>, 2014.

16 [Noël, B., van de Berg, W. J., Lhermitte, S., Wouters, B., Machguth, H., Howat, I., Citterio, M., Moholdt, G., Lenaerts, J. T.](https://doi.org/10.1038/ncomms14730)
17 [M., and van den Broeke, M. R.: A tipping point in refreezing accelerates mass loss of Greenland’s glaciers and ice caps, *Nat*](https://doi.org/10.1038/ncomms14730)
18 [Commun.](https://doi.org/10.1038/ncomms14730), 8, 14730, <https://doi.org/10.1038/ncomms14730>, 2017.

19 [Noël, B., Berg, W. J. van de, Lhermitte, S., and van den Broeke, M. R.: Rapid ablation zone expansion amplifies north](https://doi.org/10.1126/sciadv.aaw0123)
20 [Greenland mass loss, *Science Advances*, 5, eaaw0123, https://doi.org/10.1126/sciadv.aaw0123, 2019.](https://doi.org/10.1126/sciadv.aaw0123)

21 [Noël, B., van Kampenhout, L., Lenaerts, J. T. M., van de Berg, W. J., and van den Broeke, M. R.: A 21st Century Warming](https://doi.org/10.1029/2020GL090471)
22 [Threshold for Sustained Greenland Ice Sheet Mass Loss, *Geophysical Research Letters*, 48, e2020GL090471,](https://doi.org/10.1029/2020GL090471)
23 [https://doi.org/10.1029/2020GL090471, 2021.](https://doi.org/10.1029/2020GL090471)

24 [Ogi, M. and Wallace, J. M.: Summer minimum Arctic sea ice extent and the associated summer atmospheric circulation,](https://doi.org/10.1029/2007GL029897)
25 [Geophysical Research Letters](https://doi.org/10.1029/2007GL029897), 34, <https://doi.org/10.1029/2007GL029897>, 2007.

26 [Orsi, A. J., Kawamura, K., Masson-Delmotte, V., Fettweis, X., Box, J. E., Dahl-Jensen, D., Clow, G. D., Landais, A., and](https://doi.org/10.1002/2016GL072212)
27 [Severinghaus, J. P.: The recent warming trend in North Greenland, *Geophysical Research Letters*, 44, 6235–6243,](https://doi.org/10.1002/2016GL072212)
28 [https://doi.org/10.1002/2016GL072212, 2017.](https://doi.org/10.1002/2016GL072212)

29 [Otosaka, I. N., Shepherd, A., Ivins, E. R., Schlegel, N.-J., Amory, C., van den Broeke, M. R., Horwath, M., Joughin, I., King,](https://doi.org/10.5194/essd-15-1597-2023)
30 [M. D., Krinner, G., Nowicki, S., Payne, A. J., Rignot, E., Scambos, T., Simon, K. M., Smith, B. E., Sørensen, L. S., Velicogna,](https://doi.org/10.5194/essd-15-1597-2023)
31 [L., Whitehouse, P. L., A. G., Agosta, C., Ahlstrøm, A. P., Blazquez, A., Colgan, W., Engdahl, M. E., Fettweis, X., Forsberg,](https://doi.org/10.5194/essd-15-1597-2023)
32 [R., Gallée, H., Gardner, A., Gilbert, L., Gourmelen, N., Groh, A., Gunter, B. C., Harig, C., Helm, V., Khan, S. A., Kittel, C.,](https://doi.org/10.5194/essd-15-1597-2023)
33 [Konrad, H., Langen, P. L., Lecavalier, B. S., Liang, C.-C., Loomis, B. D., McMillan, M., Melini, D., Mermild, S. H., Mottram,](https://doi.org/10.5194/essd-15-1597-2023)
34 [R., Mouginot, J., Nilsson, J., Noël, B., Pattle, M. E., Peltier, W. R., Pie, N., Roca, M., Sasgen, I., Save, H. V., Seo, K.-W.,](https://doi.org/10.5194/essd-15-1597-2023)
35 [Scheuchl, B., Schrama, E. J. O., Schröder, L., Simonsen, S. B., Slater, T., Spada, G., Sutterley, T. C., Vishwakarma, B. D.,](https://doi.org/10.5194/essd-15-1597-2023)
36 [van Wessem, J. M., Wiese, D., van der Wal, W., and Wouters, B.: Mass balance of the Greenland and Antarctic ice sheets](https://doi.org/10.5194/essd-15-1597-2023)
37 [from 1992 to 2020, *Earth System Science Data*, 15, 1597–1616, https://doi.org/10.5194/essd-15-1597-2023, 2023.](https://doi.org/10.5194/essd-15-1597-2023)

38 [Overland, J. E., Francis, J. A., Hanna, E., and Wang, M.: The recent shift in early summer Arctic atmospheric circulation,](https://doi.org/10.1029/2012GL053268)
39 [Geophysical Research Letters](https://doi.org/10.1029/2012GL053268), 39, L19804, <https://doi.org/10.1029/2012GL053268>, 2012.

40 [Pedersen, R. A. and Christensen, J. H.: Attributing Greenland Warming Patterns to Regional Arctic Sea Ice Loss, *Geophysical*](#)
41 [Research Letters](#), 46, 10495–10503, <https://doi.org/10.1029/2019GL083828>, 2019.

42 [Pithan, F. and Mauritsen, T.: Arctic amplification dominated by temperature feedbacks in contemporary climate models,](#)
43 [Nature Geosci.](#) 7, 181–184, <https://doi.org/10.1038/ngeo2071>, 2014.

44 [Preece, J., Alexander, P., Mote, T., Kooperman, G., Fettweis, X., and Tedesco, M.: Modèle Atmosphérique Régional \(MAR\)](#)
45 [version 3.12 regional climate model pseudo-global warming experiment output, 2000-2019, Greenland domain, 20 kilometer](#)
46 [\(km\) horizontal resolution.,](#) <https://doi.org/10.18739/A2TT4FV6W>, 2023a.

47 [Preece, J. R., Wachowicz, L. J., Mote, T. L., Tedesco, M., and Fettweis, X.: Summer Greenland Blocking Diversity and Its](#)
48 [Impact on the Surface Mass Balance of the Greenland Ice Sheet, *Journal of Geophysical Research: Atmospheres*,](#) 127,
49 [e2021JD035489.](#) <https://doi.org/10.1029/2021JD035489>, 2022.

50 [Preece, J. R., Mote, T. L., Cohen, J., Wachowicz, L. J., Knox, J. A., Tedesco, M., and Kooperman, G. J.: Summer atmospheric](#)
51 [circulation over Greenland in response to Arctic amplification and diminished spring snow cover, *Nat Commun*,](#) 14, 3759,
52 [https://doi.org/10.1038/s41467-023-39466-6](#), 2023b.

53 [Rantanen, M., Karpechko, A. Y., Lipponen, A., Nordling, K., Hyvärinen, O., Ruosteenoja, K., Vihma, T., and Laaksonen, A.:](#)
54 [The Arctic has warmed nearly four times faster than the globe since 1979, *Commun Earth Environ*,](#) 3, 1–10,
55 [https://doi.org/10.1038/s43247-022-00498-3](#), 2022.

56 [Rasmussen, K. L., Prein, A. F., Rasmussen, R. M., Ikeda, K., and Liu, C.: Changes in the convective population and](#)
57 [thermodynamic environments in convection-permitting regional climate simulations over the United States, *Clim Dyn*,](#) 55,
58 [383–408.](#) <https://doi.org/10.1007/s00382-017-4000-7>, 2020.

59 [Rasmussen, R., Liu, C., Ikeda, K., Gochis, D., Yates, D., Chen, F., Tewari, M., Barlage, M., Dudhia, J., Yu, W., Miller, K.,](#)
60 [Arsenault, K., Grubišić, V., Thompson, G., and Gutmann, E.: High-Resolution Coupled Climate Runoff Simulations of](#)
61 [Seasonal Snowfall over Colorado: A Process Study of Current and Warmer Climate, *J. Climate*,](#) 24, 3015–3048,
62 [https://doi.org/10.1175/2010JCLI3985.1](#), 2011.

63 [Rennermalm, A. K., Smith, L. C., Stroeve, J. C., and Chu, V. W.: Does sea ice influence Greenland ice sheet surface-melt?,](#)
64 [Environ. Res. Lett.](#), 4, 024011, <https://doi.org/10.1088/1748-9326/4/2/024011>, 2009.

65 [Rogers, J. C., Bathke, D. J., Mosley-Thompson, E., and Wang, S.-H.: Atmospheric circulation and cyclone frequency](#)
66 [variations linked to the primary modes of Greenland snow accumulation, *Geophysical Research Letters*,](#) 31,
67 [https://doi.org/10.1029/2004GL021048](#), 2004.

68 [Schär, C., Frei, C., Lüthi, D., and Davies, H. C.: Surrogate climate-change scenarios for regional climate models, *Geophys.*](#)
69 [Res. Lett.](#), 23, 669–672, <https://doi.org/10.1029/96GL00265>, 1996.

70 [Schoof, C.: Ice-sheet acceleration driven by melt supply variability, *Nature*,](#) 468, 803–806,
71 [https://doi.org/10.1038/nature09618](#), 2010.

72 [Schuenemann, K. C., Cassano, J. J., and Finniss, J.: Synoptic Forcing of Precipitation over Greenland: Climatology for 1961–](#)
73 [99, *Journal of Hydrometeorology*,](#) 10, 60–78, <https://doi.org/10.1175/2008JHM1014.1>, 2009.

74 [Screen, J. A.: Influence of Arctic sea ice on European summer precipitation, *Environ. Res. Lett.*,](#) 8, 044015,
75 [https://doi.org/10.1088/1748-9326/8/4/044015](#), 2013.

76 [Screen, J. A.: Far-flung effects of Arctic warming, *Nature Geosci.* 10, 253–254, <https://doi.org/10.1038/ngeo2924>, 2017.](https://doi.org/10.1038/ngeo2924)

77 [Screen, J. A. and Simmonds, I.: The central role of diminishing sea ice in recent Arctic temperature amplification, *Nature*, 464,](https://doi.org/10.1038/nature09051)
78 [1334–1337, <https://doi.org/10.1038/nature09051>, 2010.](https://doi.org/10.1038/nature09051)

79 [Sellevold, R., Lenaerts, J. T. M., and Vizcaino, M.: Influence of Arctic sea-ice loss on the Greenland ice sheet climate, *Clim*
80 \[Dyn.\]\(https://doi.org/10.1007/s00382-021-05897-4\) 58, 179–193, <https://doi.org/10.1007/s00382-021-05897-4>, 2022.](https://doi.org/10.1007/s00382-021-05897-4)

81 [Serreze, M. C. and Barry, R. G.: Processes and impacts of Arctic amplification: A research synthesis, *Global and Planetary*
82 \[Change\]\(https://doi.org/10.1016/j.gloplacha.2011.03.004\), 77, 85–96, <https://doi.org/10.1016/j.gloplacha.2011.03.004>, 2011.](https://doi.org/10.1016/j.gloplacha.2011.03.004)

83 [Shea, D., Hurrell, J., and Phillips, A.: Merged Hadley-OI sea surface temperature and sea ice concentration data set,
84 <https://doi.org/10.5065/R33V-SV91>, 2020.](https://doi.org/10.5065/R33V-SV91)

85 [Smith, B., Fricker, H. A., Gardner, A. S., Medley, B., Nilsson, J., Paolo, F. S., Holschuh, N., Adusumilli, S., Brunt, K., Csatho,
86 \[B., Harbeck, K., Markus, T., Neumann, T., Siegfried, M. R., and Zwally, H. J.: Pervasive ice sheet mass loss reflects competing\]\(https://doi.org/10.1126/science.aaz5845\)
87 \[ocean and atmosphere processes, *Science*, 368, 1239–1242, <https://doi.org/10.1126/science.aaz5845>, 2020.\]\(https://doi.org/10.1126/science.aaz5845\)](https://doi.org/10.1126/science.aaz5845)

88 [Stroeve, J. C., Mioduszewski, J. R., Rennermalm, A., Boisvert, L. N., Tedesco, M., and Robinson, D.: Investigating the local-
89 \[scale influence of sea ice on Greenland surface melt, *The Cryosphere*, 11, 2363–2381, \\[2017\\]\\(https://doi.org/10.5194/tc-11-2363-
90 <a href=\\), 2017.\]\(https://doi.org/10.5194/tc-11-2363-2017\)](https://doi.org/10.5194/tc-11-2363-2017)

91 [Tedesco, M. and Fettweis, X.: Unprecedented atmospheric conditions \(1948–2019\) drive the 2019 exceptional melting season
92 \[over the Greenland ice sheet, *Cryosphere*, 14, 1209–1223, <https://doi.org/10.5194/tc-14-1209-2020>, 2020.\]\(https://doi.org/10.5194/tc-14-1209-2020\)](https://doi.org/10.5194/tc-14-1209-2020)

93 [Tedesco, M., Mote, T., Fettweis, X., Hanna, E., Jeyaratnam, J., Booth, J. F., Datta, R., and Briggs, K.: Arctic cut-off high
94 \[drives the poleward shift of a new Greenland melting record, *Nat Commun.* 7, 11723, <https://doi.org/10.1038/ncomms11723>,\]\(https://doi.org/10.1038/ncomms11723\)
95 \[2016.\]\(https://doi.org/10.1038/ncomms11723\)](https://doi.org/10.1038/ncomms11723)

96 [The IMBIE team, Shepherd, A., Ivins, E., Rignot, E., Smith, B., van den Broeke, M., Velicogna, I., Whitehouse, P., Briggs,
97 \[K., Joughin, I., Krinner, G., Nowicki, S., Payne, T., Scambos, T., Schlegel, N., A. G., Agosta, C., Ahlström, A., Babonis, G.,\]\(https://doi.org/10.1038/s41586-018-0179-y\)
98 \[Barletta, V., Blazquez, A., Bonin, J., Csatho, B., Cullather, R., Felikson, D., Fettweis, X., Forsberg, R., Gallee, H., Gardner,\]\(https://doi.org/10.1038/s41586-018-0179-y\)
99 \[A., Gilbert, L., Groh, A., Gunter, B., Hanna, E., Harig, C., Helm, V., Horvath, A., Horvath, M., Khan, S., Kjeldsen, K. K.,\]\(https://doi.org/10.1038/s41586-018-0179-y\)
00 \[Konrad, H., Langen, P., Lecavalier, B., Loomis, B., Luthcke, S., McMillan, M., Melini, D., Memild, S., Mohajerani, Y., Moore,\]\(https://doi.org/10.1038/s41586-018-0179-y\)
01 \[P., Mouginit, J., Moyano, G., Muir, A., Nagler, T., Nield, G., Nilsson, J., Noel, B., Ootaka, I., Pattle, M. E., Peltier, W. R.,\]\(https://doi.org/10.1038/s41586-018-0179-y\)
02 \[Pie, N., Rietbroek, R., Rott, H., Sandberg-Sørensen, L., Sasgen, I., Save, H., Scheuchl, B., Schrama, E., Schröder, L., Seo, K.-\]\(https://doi.org/10.1038/s41586-018-0179-y\)
03 \[W., Simonsen, S., Slater, T., Spada, G., Sutterley, T., Talpe, M., Tarasov, L., van de Berg, W. J., van der Wal, W., van Wessem,\]\(https://doi.org/10.1038/s41586-018-0179-y\)
04 \[M., Vishwakarma, B. D., Wiese, D., and Wouters, B.: Mass balance of the Antarctic Ice Sheet from 1992 to 2017, *Nature*,\]\(https://doi.org/10.1038/s41586-018-0179-y\)
05 \[558, 219–222, <https://doi.org/10.1038/s41586-018-0179-y>, 2018.\]\(https://doi.org/10.1038/s41586-018-0179-y\)](https://doi.org/10.1038/s41586-018-0179-y)

06 [The IMBIE Team, Shepherd, A., Ivins, E., Rignot, E., Smith, B., van den Broeke, M., Velicogna, I., Whitehouse, P., Briggs,
07 \[K., Joughin, I., Krinner, G., Nowicki, S., Payne, T., Scambos, T., Schlegel, N., A. G., Agosta, C., Ahlström, A., Babonis, G.,\]\(https://doi.org/10.1038/s41586-018-0179-y\)
08 \[Barletta, V. R., Bjørk, A. A., Blazquez, A., Bonin, J., Colgan, W., Csatho, B., Cullather, R., Engdahl, M. E., Felikson, D.,\]\(https://doi.org/10.1038/s41586-018-0179-y\)
09 \[Fettweis, X., Forsberg, R., Hogg, A. E., Gallee, H., Gardner, A., Gilbert, L., Gourmelen, N., Groh, A., Gunter, B., Hanna, E.,\]\(https://doi.org/10.1038/s41586-018-0179-y\)
10 \[Harig, C., Helm, V., Horvath, A., Horvath, M., Khan, S., Kjeldsen, K. K., Konrad, H., Langen, P. L., Lecavalier, B., Loomis,\]\(https://doi.org/10.1038/s41586-018-0179-y\)
11 \[B., Luthcke, S., McMillan, M., Melini, D., Memild, S., Mohajerani, Y., Moore, P., Mottram, R., Mouginit, J., Moyano, G.,\]\(https://doi.org/10.1038/s41586-018-0179-y\)
12 \[Muir, A., Nagler, T., Nield, G., Nilsson, J., Noël, B., Ootaka, I., Pattle, M. E., Peltier, W. R., Pie, N., Rietbroek, R., Rott, H.,\]\(https://doi.org/10.1038/s41586-018-0179-y\)
13 \[Sandberg Sørensen, L., Sasgen, I., Save, H., Scheuchl, B., Schrama, E., Schröder, L., Seo, K.-W., Simonsen, S. B., Slater, T.,\]\(https://doi.org/10.1038/s41586-018-0179-y\)
14 \[Spada, G., Sutterley, T., Talpe, M., Tarasov, L., van de Berg, W. J., van der Wal, W., van Wessem, M., Vishwakarma, B. D.,\]\(https://doi.org/10.1038/s41586-018-0179-y\)](https://doi.org/10.1038/s41586-018-0179-y)

15 [Wiese, D., Wilton, D., Wagner, T., Wouters, B., and Wuite, J.: Mass balance of the Greenland Ice Sheet from 1992 to 2018,](#)
16 [Nature, 579, 233–239, <https://doi.org/10.1038/s41586-019-1855-2>, 2020.](#)

17 [Topál, D., Ding, Q., Ballinger, T. J., Hanna, E., Fettweis, X., Li, Z., and Pieczka, I.: Discrepancies between observations and](#)
18 [climate models of large-scale wind-driven Greenland melt influence sea-level rise projections, Nat Commun, 13,](#)
19 [https://doi.org/10.1038/s41467-022-34414-2, 2022.](#)

20 [Trenberth, K. E.: Changes in precipitation with climate change, Climate Research, 47, 123–138, 2011.](#)

21 [Trenberth, K. E., Fasullo, J. T., and Shepherd, T. G.: Attribution of climate extreme events, Nature Clim Change, 5, 725–730,](#)
22 [https://doi.org/10.1038/nclimate2657, 2015.](#)

23 [Vavrus, S. J., Wang, F., Martin, J. E., Francis, J. A., Peings, Y., and Cattiaux, J.: Changes in North American Atmospheric](#)
24 [Circulation and Extreme Weather: Influence of Arctic Amplification and Northern Hemisphere Snow Cover, J. Climate, 30,](#)
25 [4317–4333, <https://doi.org/10.1175/JCLI-D-16-0762.1>, 2017.](#)

26 [Velicogna, I., Mohajerani, Y., A. G., Landerer, F., Mougnot, J., Noel, B., Rignot, E., Sutterley, T., van den Broeke, M., van](#)
27 [Wessem, M., and Wiese, D.: Continuity of Ice Sheet Mass Loss in Greenland and Antarctica From the GRACE and GRACE](#)
28 [Follow-On Missions, Geophysical Research Letters, 47, e2020GL087291, <https://doi.org/10.1029/2020GL087291>, 2020.](#)

29 [Wang, S., Ma, X., Zhou, S., Wu, L., Wang, H., Tang, Z., Xu, G., Jing, Z., Chen, Z., and Gan, B.: Extreme atmospheric rivers](#)
30 [in a warming climate, Nat Commun, 14, 3219, <https://doi.org/10.1038/s41467-023-38980-x>, 2023.](#)

31 [Wang, W., Zender, C. S., and As, D. van: Temporal Characteristics of Cloud Radiative Effects on the Greenland Ice Sheet:](#)
32 [Discoveries From Multiyear Automatic Weather Station Measurements, Journal of Geophysical Research: Atmospheres, 123,](#)
33 [11,348–11,361, <https://doi.org/10.1029/2018JD028540>, 2018.](#)

34 [Wang, W., Zender, C. S., As, D. van, and Miller, N. B.: Spatial Distribution of Melt Season Cloud Radiative Effects Over](#)
35 [Greenland: Evaluating Satellite Observations, Reanalyses, and Model Simulations Against In Situ Measurements, Journal of](#)
36 [Geophysical Research: Atmospheres, 124, 57–71, <https://doi.org/10.1029/2018JD028919>, 2019.](#)

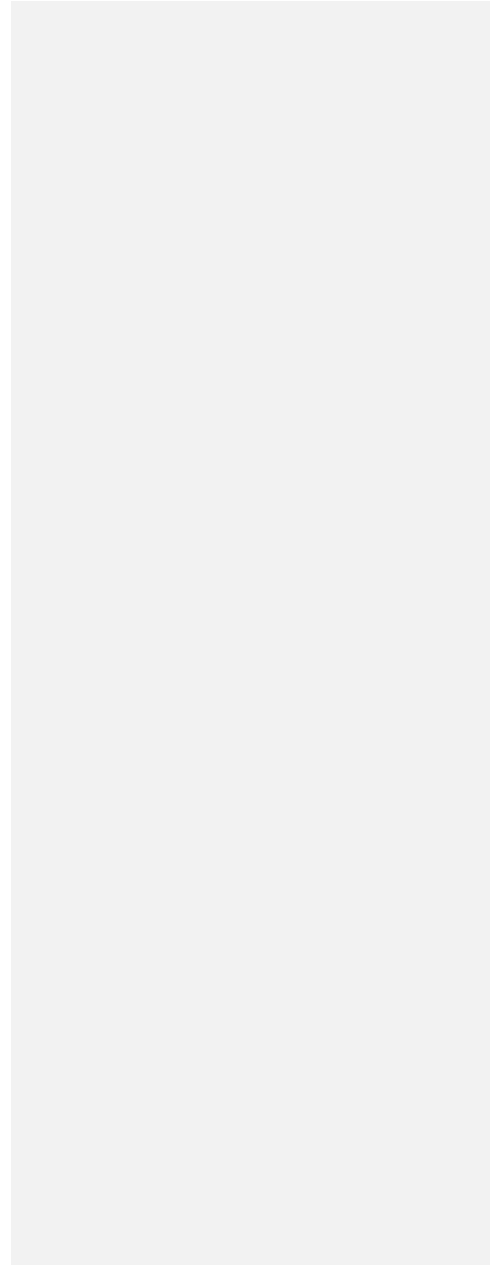
37 [Wilcoxon, F.: Individual Comparisons by Ranking Methods, Biometrics Bulletin, 1, 80–83, <https://doi.org/10.2307/3001968>,](#)
38 [1945.](#)

39 [Woollings, T., Barriopedro, D., Methven, J., Son, S.-W., Martius, O., Harvey, B., Sillmann, J., Lupo, A. R., and Seneviratne,](#)
40 [S.: Blocking and its Response to Climate Change, Curr Clim Change Rep, 4, 287–300, <https://doi.org/10.1007/s40641-018->](#)
41 [0108-z, 2018.](#)

42 [Wu, B., Zhang, R., D'Arrigo, R., and Su, J.: On the Relationship between Winter Sea Ice and Summer Atmospheric Circulation](#)
43 [over Eurasia, J. Climate, 26, 5523–5536, <https://doi.org/10.1175/JCLI-D-12-00524.1>, 2013.](#)

44 [Yang, C., Leonelli, F. E., Marullo, S., Artale, V., Beggs, H., Nardelli, B. B., Chin, T. M., Toma, V. D., Good, S., Huang, B.,](#)
45 [Merchant, C. J., Sakurai, T., Santoleri, R., Vazquez-Cuervo, J., Zhang, H.-M., and Pisano, A.: Sea Surface Temperature](#)
46 [Intercomparison in the Framework of the Copernicus Climate Change Service \(C3S\), Journal of Climate, 34, 5257–5283,](#)
47 [https://doi.org/10.1175/JCLI-D-20-0793.1, 2021.](#)

48 [Zemp, M., Huss, M., Thibert, E., Eckert, N., McNabb, R., Huber, J., Barandun, M., Machguth, H., Nussbaumer, S. U., Gärtner-](#)
49 [Roer, I., Thomson, L., Paul, F., Maussion, F., Kutuzov, S., and Cogley, J. G.: Global glacier mass changes and their](#)
50 [contributions to sea-level rise from 1961 to 2016, Nature, 568, 382–386, <https://doi.org/10.1038/s41586-019-1071-0>, 2019.](#)



Page 16: [1] Formatted	Jonathon Preece	12/31/25 5:50:00 PM
-------------------------------	------------------------	----------------------------

Font: 10 pt

Page 16: [1] Formatted	Jonathon Preece	12/31/25 5:50:00 PM
-------------------------------	------------------------	----------------------------

Font: 10 pt

Page 16: [1] Formatted	Jonathon Preece	12/31/25 5:50:00 PM
-------------------------------	------------------------	----------------------------

Font: 10 pt

Page 16: [2] Formatted	Jonathon Preece	12/31/25 5:58:00 PM
-------------------------------	------------------------	----------------------------

Font: 10 pt

Page 16: [2] Formatted	Jonathon Preece	12/31/25 5:58:00 PM
-------------------------------	------------------------	----------------------------

Font: 10 pt

Page 16: [3] Formatted	Jonathon Preece	12/31/25 5:50:00 PM
-------------------------------	------------------------	----------------------------

Font: 10 pt

Page 16: [3] Formatted	Jonathon Preece	12/31/25 5:50:00 PM
-------------------------------	------------------------	----------------------------

Font: 10 pt

Page 16: [3] Formatted	Jonathon Preece	12/31/25 5:50:00 PM
-------------------------------	------------------------	----------------------------

Font: 10 pt

Page 16: [4] Formatted	Jonathon Preece	12/31/25 5:58:00 PM
-------------------------------	------------------------	----------------------------

Font: 10 pt

Page 16: [4] Formatted	Jonathon Preece	12/31/25 5:58:00 PM
-------------------------------	------------------------	----------------------------

Font: 10 pt

Page 16: [5] Formatted	Jonathon Preece	12/31/25 5:50:00 PM
-------------------------------	------------------------	----------------------------

Font: 10 pt

Page 16: [5] Formatted	Jonathon Preece	12/31/25 5:50:00 PM
-------------------------------	------------------------	----------------------------

Font: 10 pt

Page 16: [5] Formatted	Jonathon Preece	12/31/25 5:50:00 PM
-------------------------------	------------------------	----------------------------

Font: 10 pt

Page 16: [6] Formatted	Jonathon Preece	12/31/25 5:58:00 PM
-------------------------------	------------------------	----------------------------

Font: 10 pt

Page 16: [6] Formatted	Jonathon Preece	12/31/25 5:58:00 PM
-------------------------------	------------------------	----------------------------

Font: 10 pt

Page 18: [7] Deleted	Jonathon Preece	2/22/26 11:42:00 PM
-----------------------------	------------------------	----------------------------

▼

Page 18: [8] Deleted	Jonathon Ralph Preece	3/9/26 2:24:00 PM
-----------------------------	------------------------------	--------------------------

▼

Page 18: [9] Deleted	Jonathon Ralph Preece	3/9/26 2:27:00 PM
-----------------------------	------------------------------	--------------------------

▼

Page 18: [10] Deleted	Jonathon Preece	2/23/26 12:09:00 AM
------------------------------	------------------------	----------------------------

▼

Page 20: [11] Formatted	Jonathon Preece	12/31/25 5:53:00 PM
--------------------------------	------------------------	----------------------------

Font: 10 pt

Page 20: [11] Formatted	Jonathon Preece	12/31/25 5:53:00 PM
--------------------------------	------------------------	----------------------------

Font: 10 pt

Page 20: [11] Formatted	Jonathon Preece	12/31/25 5:53:00 PM
--------------------------------	------------------------	----------------------------

Font: 10 pt

Page 20: [12] Formatted	Jonathon Preece	12/31/25 6:00:00 PM
--------------------------------	------------------------	----------------------------

Font: 10 pt

Page 20: [12] Formatted	Jonathon Preece	12/31/25 6:00:00 PM
--------------------------------	------------------------	----------------------------

Font: 10 pt

Page 20: [13] Formatted	Jonathon Preece	12/31/25 5:53:00 PM
--------------------------------	------------------------	----------------------------

Font: 10 pt

Page 20: [13] Formatted	Jonathon Preece	12/31/25 5:53:00 PM
--------------------------------	------------------------	----------------------------

Font: 10 pt

Page 20: [13] Formatted	Jonathon Preece	12/31/25 5:53:00 PM
--------------------------------	------------------------	----------------------------

Font: 10 pt

Page 20: [14] Formatted	Jonathon Preece	12/31/25 6:00:00 PM
--------------------------------	------------------------	----------------------------

Font: 10 pt

Page 20: [14] Formatted	Jonathon Preece	12/31/25 6:00:00 PM
--------------------------------	------------------------	----------------------------

Font: 10 pt

Page 20: [15] Deleted **Jonathon Ralph Preece** **3/9/26 10:49:00 AM**

▼

Page 20: [15] Deleted **Jonathon Ralph Preece** **3/9/26 10:49:00 AM**

▼

Page 20: [16] Deleted **Jonathon Ralph Preece** **3/9/26 2:47:00 PM**

▼

Page 20: [16] Deleted **Jonathon Ralph Preece** **3/9/26 2:47:00 PM**

▼

Page 20: [17] Deleted **Jonathon Ralph Preece** **3/9/26 2:48:00 PM**

▼

Page 20: [17] Deleted **Jonathon Ralph Preece** **3/9/26 2:48:00 PM**

▼

Page 20: [18] Deleted **Jonathon Ralph Preece** **3/9/26 2:52:00 PM**

▼

Page 24: [19] Formatted **Jonathon Preece** **12/31/25 5:54:00 PM**

Font: 10 pt

Page 24: [19] Formatted **Jonathon Preece** **12/31/25 5:54:00 PM**

Font: 10 pt

Page 24: [19] Formatted **Jonathon Preece** **12/31/25 5:54:00 PM**

Font: 10 pt

Page 24: [20] Formatted **Jonathon Preece** **12/31/25 5:59:00 PM**

Font: 10 pt

Page 24: [20] Formatted **Jonathon Preece** **12/31/25 5:59:00 PM**

Font: 10 pt

Page 24: [21] Formatted **Jonathon Preece** **12/31/25 5:54:00 PM**

Font: 10 pt

Page 24: [21] Formatted **Jonathon Preece** **12/31/25 5:54:00 PM**

Font: 10 pt

Page 24: [21] Formatted **Jonathon Preece** **12/31/25 5:54:00 PM**

Font: 10 pt

Page 24: [22] Formatted

Jonathon Preece

12/31/25 5:59:00 PM

Font: 10 pt

Page 24: [22] Formatted

Jonathon Preece

12/31/25 5:59:00 PM

Font: 10 pt